

Vacuum-induced surface-acoustic-wave phonon blockade

Jiangshan Tang,^{1,2,3,*} Yang Wu,^{2,4,*} Zhenkai Wang,^{1,3} Hui Sun^{①,4,†} Lei Tang,^{1,2} Han Zhang^{①,1,3}
 Tao Li,⁵ Yanqin Lu (陆延青),^{1,2,‡} Min Xiao (肖敏),^{1,2,3,6} and Keyu Xia (夏可宇)^{①,1,2,3,7,§}

¹*National Laboratory of Solid State Microstructures, Collaborative Innovation Center of Advanced Microstructures, Nanjing University, Nanjing 210093, China*

²*College of Engineering and Applied Sciences, Nanjing University, Nanjing 210093, China*

³*School of Physics, Nanjing University, Nanjing 210093, China*

⁴*School of Physics and Information Technology, Shaanxi Normal University, Xi'an 710062, China*

⁵*School of Science, Nanjing University of Science and Technology, Nanjing 210094, China*

⁶*Department of Physics, University of Arkansas, Fayetteville, Arkansas 72701, USA*

⁷*Jiangsu Key Laboratory of Artificial Functional Materials, and Key Laboratory of Intelligent Optical Sensing and Manipulation, Ministry of Education, Nanjing University, Nanjing 210093, China*



(Received 1 July 2019; accepted 30 March 2020; published 1 May 2020)

Photon blockade via a giant self-Kerr nonlinearity in an optical resonator induced by an N-type quantum system is one of the main routines towards photon-based quantum information processing. However, such an N-type system for phonons is lacking. We propose an effective N-type quantum system for phonons, forming from a superconducting transmon qubit and a microwave resonator. In the absence of any external driving, the quantum vacuum-qubit interaction causes the surface acoustic wave (SAW) phonon blockade. Such a vacuum-induced phonon blockade paves the way to prepare single SAW phonons from a weak coherent phononic state for SAW accessible superconducting quantum computation.

DOI: [10.1103/PhysRevA.101.053802](https://doi.org/10.1103/PhysRevA.101.053802)

I. INTRODUCTION

A superconducting quantum circuit (SQC) is one of the most promising candidates for scalable quantum computation [1–4]. SQCs have the capabilities of entangling multipartite qubits [5], solving linear equations [6], cooling nanomechanical resonators [7–9], and quantum walk [10].

Typically, SQCs are accessed by microwave (MW) fields. However, the MW crosstalk is an inevitable issue when SQCs continue to scale up, due to the large MW wavelength and radiation [11,12]. To tackle this crosstalk issue, surface acoustic wave (SAW) phonons are successfully used to manipulate SQCs very recently [13–17], thanks to the small wavelength and the absence of radiation. Because of these merits of SAWs, hybrid quantum systems consisting of SAWs and SQCs, in particular, superconducting transmon qubits, have received intensive attention [13–20]. The superconducting transmon qubit is treated as an ideal bridge for constructing the hybrid quantum system due to its long dephasing time and immunity to charge noise [2,3,21–26], and its capability of electrically coupling to a SAW. The experimental and theoretical progresses in hybrid SAW-SQC quantum systems lead to the emergence of the so-called “circuit quantum acoustodynamics” [27–30]. Recent experiments have demonstrated that a SAW can also interact with electronic spins [31,32].

Therefore, a SAW has become a candidate for building a hybrid quantum interface between SQCs and optical photons in mediate of spins. However, the control of SAW phonons in phonon-based quantum systems is not as mature as that of photons. Manipulation of a single SAW phonon such as a phonon blockade can provide versatile manners for phonon-based quantum information processing.

Photonic Kerr nonlinearities have been intensively studied for control of the propagation of photons, allowing photon delay [33,34] and photonic chirality [35,36]. Apart from an atom-cavity system [37], photon blockade can also be achieved by using photonic Kerr nonlinearities [38–43]. In stark contrast, phonon Kerr nonlinearity and blockade have only been discussed for trapped ions [44] or “static phonons” in micromechanical resonators vibrating at low frequency [45–51]. An N-type quantum system is extensively used to create a giant Kerr nonlinearity for photons [33,36,52–59] and thus is highly demanded for photon blockade and transport [38–41,60]. However, such an N-type system for SAW phonons with high frequency is so far elusive. Below, we will propose an experimentally feasible scheme for quantum vacuum-induced blockade of SAW phonons.

The quantum vacuum field is a basic concept of quantum physics, which is of great significance in fundamental physics and importance to quantum technology [61,62]. Due to the limitation of experimental technology, it has been difficult to study the vacuum field before. With the recent progress of quantum technology, the unique nature of quantum vacuum field has been continuously revealed and its applications as a quantum resource have been exploited [63–67]. Our proposal makes full use of the quantum vacuum field to achieve a

*These authors contributed equally to this work.

†physunh@snnu.edu.cn

‡qylu@nju.edu.cn

§keyu.xia@nju.edu.cn

phonon blockade in a SAW-superconducting hybrid quantum chip. It may provide an on-chip platform for studying the quantum vacuum field.

In this paper, we construct an N-type artificial atom for SAW phonons using a SAW-SQC hybrid quantum system. Further, we propose two methods for blockade of propagating SAW phonons: (i) The SAW phonon blockade results from a large self-Kerr nonlinearity, created by the strong interaction between the superconducting qubit and the vacuum field in a MW resonator. (ii) The vacuum-qubit coupling causes bound states for a propagating SAW, leading to phonon blockade.

This paper is organized as following: In Sec. II, we exploit the interaction of the quantum vacuum field of a microwave resonator and a superconducting qubit to realize an effective N-type four-level system. Using this N-type system, we propose a way to create the vacuum-induced giant self-Kerr phononic nonlinearity in the resonator-qubit-resonator (RQR) system and the vacuum-induced bound states of phonons in the waveguide-qubit-resonator (WQR) system, respectively. Then, we show the SAW phonon blockade in these two kinds of systems and calculate the SAW-phonon statistics, indicated by the second-order correlation functions in Sec. III. Moreover, we also present the corresponding transmission. In the end, we present a feasible implementation of our schemes in Sec. IV, and discussion and conclusion of our work in Sec. V.

II. SYSTEM AND MODEL

In photonic systems, natural atoms with four-level structures are widely used to achieve the photon blockade by coupling to optical cavities or waveguides [38–41,53,68]. However, a phononic version of such four-level systems is elusive. Below we propose a scheme to construct an efficient N-type four-level system coupled to a phonon resonator or a phonon waveguide. With this N-type system, we first present the vacuum-induced giant self-Kerr phononic nonlinearity in a RQR system. Then, we show the phononic bound states in a WQR system.

A. Two-level model of the superconducting qubit

In experiment, the superconducting transmon qubit has a few ladder quantum states, the ground state $|g\rangle$ with energy ω_g , the first excited state $|e\rangle$ with energy ω_e , and the second excited state $|f\rangle$ with energy ω_f . For simplicity, we take $\omega_g = 0$ below. In our schemes, the MW resonator is in the quantum vacuum state. The qubit is mostly excited by the weak SAW phonon. As we can see below, because the phonon-qubit coupling is much weaker than the MW-qubit one, the excitation of the state $|e\rangle$ is negligible, and that of $|f\rangle$ is even smaller. Moreover, a superconducting transmon qubit can be engineered to have a large enough anharmonicity $\alpha = \omega_f - 2\omega_e$, typically, $\alpha/2\pi \sim 200 - 300$ MHz [17,69]. Thus, the qubit anharmonicity can be much larger than the field-qubit coupling and the decay rate γ of the state $|e\rangle$, also the bandwidth of SAW phonons involved in our schemes. In this case, it is reasonable to treat the transmon qubit, to a good approximation as a two-level system only involving the ground and excited states, $|g\rangle$ and $|e\rangle$ [14,28–30,69–73].

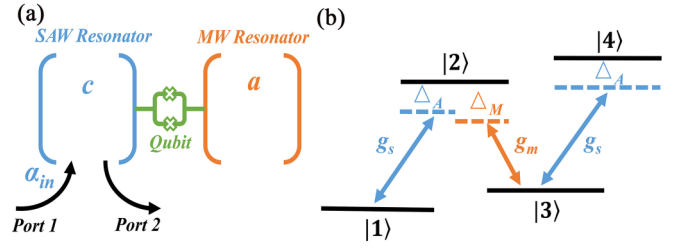


FIG. 1. Schematic diagram of the hybrid quantum system of cavity types for the SAW phonon blockade. (a) Schematic of the resonator-qubit-resonator (RQR) system. A superconducting transmon qubit couples to a SAW resonator and a MW resonator. g_s (g_m) is the qubit-SAW (MW) coupling strength. (b) Effective N-type four-level system modeling this RQR hybrid quantum system. The detuning between the SAW (MW) resonator frequency and the qubit is denoted as $\Delta_A = \omega_A - \omega_e$ ($\Delta_M = \omega_m - \omega_e$).

B. Vacuum-induced giant self-Kerr phononic nonlinearity

The RQR system for the SAW phonon blockade is depicted in Fig. 1(a). The SAW resonator with resonance frequency ω_A couples to the superconducting transmon qubit. The latter simultaneously couples to the MW resonator with resonance frequency ω_m . The SAW mode \hat{c} and the qubit interact with a rate g_s . Such a RQR system has been demonstrated in experiment for detection of the SAW near the quantum limit [17]. In this RQR system, a weak coherent SAW α_{in} with frequency ω_{in} incidents from port 1 to the SAW resonator. The outgoing SAW from port 2 shows the phonon blockade. The qubit also couples to the MW resonator with a strength g_m . In this RQR system, we take $g_s, g_m \ll \alpha \sim 2\pi \times 250$ MHz that the two-level model of the superconducting qubit is valid [69]. Note that both the qubit and MW resonator have transition frequencies of several GHz and can be prepared in the ground and the vacuum states when cooled down to 20 mK.

In the case of a weak SAW probe and $g_s \ll g_m$ that the zero-photon state in the MW resonator is mostly populated, we can truncate the MW resonator up to the Fock state $|1_m\rangle$. The qubit-MW-resonator subsystem can be modeled as a four-level system with $|1\rangle = |g, 0_m\rangle$ for the vacuum state, $|2\rangle = |e, 0_m\rangle$, $|3\rangle = |g, 1_m\rangle$, and $|4\rangle = |e, 1_m\rangle$ [74] [see Fig. 1(b)]. The energies of these four states are 0, ω_e , ω_m , and $\omega_e + \omega_m$, respectively. The SAW resonator mode \hat{c} couples to the transitions $|1\rangle \leftrightarrow |2\rangle$ and $|3\rangle \leftrightarrow |4\rangle$. The MW quantum vacuum field drives the transition $|2\rangle \leftrightarrow |3\rangle$. Note that the MW-qubit subsystem is mostly populated in the state $|1\rangle$. In this case, we construct an N-type artificial atom for the SAW phonon.

For the RQR system without the probe in a rotating frame, defined by a unitary transformation $\hat{U}_1 = \exp\{i[\omega_A \hat{c}^\dagger \hat{c} + \omega_A \hat{a}^\dagger \hat{a} + \omega_A \sigma_{ee} t]\}$, the Hamiltonian takes the form ($\hbar = 1$),

$$\hat{H}_{RQR} = (\Delta_M - \Delta_A) \hat{a}^\dagger \hat{a} - \Delta_A \hat{\sigma}_{ee} + g_m (\hat{a}^\dagger \hat{\sigma}_{ge} + \hat{\sigma}_{eg} \hat{a}) + g_s (\hat{c}^\dagger \hat{\sigma}_{ge} + \hat{\sigma}_{eg} \hat{c}), \quad (1)$$

where \hat{a} is the annihilation operator of the MW resonator, and $\hat{\sigma}_{kl} \equiv |k\rangle \langle l|$ ($k, l = g, e$). We have $\Delta_A = \omega_A - \omega_e$ ($\Delta_M = \omega_m - \omega_e$), denoting the detuning between the SAW (MW) resonator and the qubit. The third (fourth) term describes the interaction of the qubit and the MW (SAW) resonator.

In the basis of $\{|1\rangle, |2\rangle, |3\rangle, |4\rangle\}$, the Hamiltonian \hat{H}_{RQR} becomes

$$\hat{H}'_{\text{RQR}} = (\Delta_M - \Delta_A)(\hat{S}_{33} + \hat{S}_{44}) - \Delta_A(\hat{S}_{22} + \hat{S}_{44}) + (g_m \hat{S}_{32} + g_s \hat{c}^\dagger \hat{S}_{12} + g_s \hat{c}^\dagger \hat{S}_{34} + \text{H.c.}), \quad (2)$$

with $\hat{S}_{mn} = |m\rangle\langle n|$ ($m, n = 1, 2, 3, 4$). Our system is very different from the previously studied N-type atomic systems for photonic Kerr nonlinearity [36,60] or the polariton blockade [51], where a strong coherent field is needed to drive the system. Instead, the external control field is replaced by the vacuum-qubit coupling in our system.

The MW vacuum field can create a giant self-Kerr nonlinearity for SAW phonons. In our case, we have $\hat{\rho}_{11} \approx 1$. We can use a perturbation approach to solve the master equation and obtain the effective self-Kerr nonlinear coefficient [36,60,75–77] (see Appendix A):

$$\eta = \frac{2ig_s^4}{\gamma g_m^4} \left(\frac{1}{F^*} - \frac{1}{F} \right) \left(\frac{1}{F} + \frac{1}{F^*} \right), \quad (3)$$

with $F = 1/[-\kappa_m/2 + i(-\Delta_A + \Delta_M)] - (\gamma/2 + \Gamma_\phi/2 + i\Delta_A)/g_m^2$. For simplicity, we set $\Gamma_\phi = 0$. The self-Kerr nonlinearity causes an energy shift $\eta \langle \hat{c}^\dagger \hat{c} \rangle^2$ in the SAW resonator, depends on its excitation $\langle \hat{c}^\dagger \hat{c} \rangle$. Now the RQR system is equivalent to a nonlinear SAW resonator.

Applying a second unitary transformation, $\hat{U}_2 = \exp[i(\omega_{\text{in}} - \omega_A)\hat{c}^\dagger \hat{c}t]$, to the RQR system with the probe, we obtain an effective Hamiltonian modeling the probe of this nonlinear SAW resonator as

$$\hat{H}_{\text{eff}} = (\tilde{\Delta} - \eta - \Delta_a)\hat{c}^\dagger \hat{c} + \eta \hat{c}^\dagger \hat{c} \hat{c}^\dagger \hat{c} + i\sqrt{2\kappa_{\text{p,e1}}}\alpha_{\text{in}}(\hat{c}^\dagger - \hat{c}), \quad (4)$$

where $\Delta_a = \omega_{\text{in}} - \omega_A$, $\kappa_{\text{p,e1}}$ is the external decay of the SAW resonator due to the coupling to the input port, α_{in} is the weak SAW phonon signal, and a linear shift $\tilde{\Delta} = (g_s^2 \Delta_A / g_m^2 \gamma)(1/F + 1/F^*) + (ig_s^2 / g_m^2)(1/F^* - 1/F)$. The output from port 2, $\hat{c}_{\text{out}} = \sqrt{2\kappa_{\text{p,e2}}}\hat{c}$, can be found according to the cavity input-output relation [78], where $\kappa_{\text{p,e2}}$ is the external decay caused by the output port.

It is instructive to look at the approximate analytical results of the self-Kerr nonlinear coefficient for selecting parameters of the numerical simulation in Sec. III. We present two cases: (i) When we consider two-phonon resonance, i.e., $\Delta_M = \Delta_A$, the effective self-Kerr nonlinear coefficient can be solved as

$$\eta \approx -4(g_s^4 \kappa_m^3 / g_m^4 \gamma)(\Delta_A / g_m^2), \quad (5)$$

from Eq. (3). If $g_m^2 \gg \Delta_A$, the value of η compared to the decay rate of the SAW resonator will become very small. (ii) In order to obtain a greater self-Kerr nonlinearity in $g_m^2 \gg \Delta_A$, we consider the case of $\Delta_M \neq \Delta_A$, the coefficient can be derived as

$$\eta \approx -4(g_s^4 / g_m^4 \gamma)(\Delta_M - \Delta_A)\kappa_m. \quad (6)$$

It can be seen from this expression that the value of η is proportional to g_s/g_m and the absolute value of $\Delta_M - \Delta_A$. We can achieve a large phononic self-Kerr nonlinearity by adjusting the values of g_s^4/g_m^4 and $|\Delta_M - \Delta_A|$. Our aim is to achieve phonon blockade with a large self-Kerr nonlinearity. Obviously, a large difference $|\Delta_M - \Delta_A|$ is preferable. The

case of a small difference between the detunings will not be considered here.

The evolution of the system can be found by solving the master equation,

$$\dot{\hat{\rho}}(t) = -i[\hat{H}_{\text{eff}}, \hat{\rho}(t)] + \kappa_p[2\hat{c}\hat{\rho}(t)\hat{c}^\dagger - \hat{c}^\dagger \hat{c}\hat{\rho}(t) - \hat{\rho}(t)\hat{c}^\dagger \hat{c}]. \quad (7)$$

The SAW resonator has three decay channels: the input and output ports, and the intrinsic decay channel leading to a decay rate $\kappa_{\text{p,i}}$. Thus, its total decay rate is $\kappa_p = \kappa_{\text{p,e1}} + \kappa_{\text{p,e2}} + \kappa_{\text{p,i}}$. We assume that $\kappa_{\text{p,e1}} = \kappa_{\text{p,e2}} = \kappa_{\text{p,e}}$. The phonon blockade using a nonlinear cavity can be derived directly from the effective Hamiltonian in Eq. (4). Once the SAW resonator absorbs an on-resonance phonon from the probe field when $\Delta_a = \tilde{\Delta}$, “eating” a second phonon requires additional 2η energy, due to the self-Kerr nonlinearity. Because of this energy mismatching, the SAW resonator is prevented from high-phonon excitation, forming a phonon blockade in the resonator. According to the standard input-output relation, the statistical properties of the output phonon mode is the same as that in the SAW resonator, and can thus be evaluated with the steady-state second-order correlation at zero delay:

$$g^{(2)}(0) = \frac{\langle \hat{c}^\dagger(t)\hat{c}^\dagger(t)\hat{c}(t)\hat{c}(t) \rangle}{\langle \hat{c}^\dagger(t)\hat{c}(t) \rangle^2}. \quad (8)$$

The outgoing phonons tend to exit the SAW resonator one by one, resulting in the sub-Poissonian distribution, if $g^{(2)}(0) < 0.5$. Here, our Kerr-nonlinear SAW resonator can achieve this goal.

Next, we present the derivation of the transmission. In our RQR system, we can get the dynamics of the SAW resonator from the effective Hamiltonian given in Eq. (4) as

$$\frac{d}{dt}\hat{c} = -i(\tilde{\Delta} - \Delta_a)\hat{c} - 2i\eta\hat{c}^\dagger \hat{c}\hat{c} + \sqrt{2\kappa_{\text{p,e1}}}\alpha_{\text{in}} - \kappa_p\hat{c}. \quad (9)$$

When adjusting the frequency of the probe field to $\tilde{\Delta} = \Delta_a$, we obtain the steady-state solution,

$$\hat{c} = \frac{\sqrt{2\kappa_{\text{p,e1}}}\alpha_{\text{in}}}{2i\eta\langle \hat{c}^\dagger \hat{c} \rangle + \kappa_p}. \quad (10)$$

Here, we assume $\hat{c}^\dagger \hat{c}\hat{c} \approx \langle \hat{c}^\dagger \hat{c} \rangle \hat{c}$ by neglecting the quantum correlation and applying the mean value approximation. According to the cavity input-output relation, $\hat{c}_{\text{out}} = \sqrt{2\kappa_{\text{p,e2}}}\hat{c}$ [78], the transmission of the system is

$$T = \frac{\langle \hat{c}_{\text{out}}^\dagger \hat{c}_{\text{out}} \rangle}{|\alpha_{\text{in}}|^2} = \frac{4\kappa_{\text{p,e}}^2}{4\eta^2 \langle \hat{c}^\dagger \hat{c} \rangle^2 + \kappa_p^2}. \quad (11)$$

We are mainly interested in the case of a weak SAW probe. Thus, the phonon number in the SAW resonator, $\langle \hat{c}^\dagger \hat{c} \rangle$, is small and can be solved by an iterative method using Eq. (10), i.e.,

$$\hat{c}_{i+1} = \frac{\sqrt{2\kappa_{\text{p,e1}}}\alpha_{\text{in}}}{2i\eta\langle \hat{c}^\dagger \hat{c} \rangle_i + \kappa_p}. \quad (12)$$

Here, the subscript i represents the i th-order approximation. We assume that $2\eta\langle \hat{c}^\dagger \hat{c} \rangle_0 \ll \kappa_p$ at the same time. Then, we get $\langle \hat{c}^\dagger \hat{c} \rangle_1 \approx (2\kappa_{\text{p,e}}/\kappa_p^2)|\alpha_{\text{in}}|^2$ and $\langle \hat{c}^\dagger \hat{c} \rangle_2 \approx$

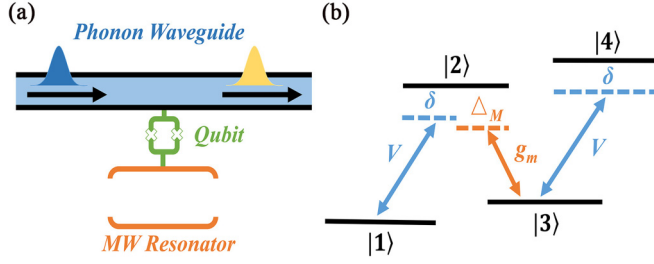


FIG. 2. Schematic diagram for the blockade of SAW phonon propagating in an 1D SAW waveguide. (a) Schematic of the waveguide-qubit-resonator (WQR) system. As in Fig. 1(a), the SAW resonator is replaced by a 1D SAW waveguide. The qubit-waveguide coupling rate is V . (b) Effective N-type four-level system modeling this WQR system. The detuning between the SAW waveguide mode and the qubit is denoted as δ . The transition $|2\rangle \leftrightarrow |3\rangle$ is coupled by the MW vacuum field with the strength g_m and detuning Δ_M .

$[2\kappa_{p,e}\kappa_p^4/(16\eta^2\kappa_{p,e}^2|\alpha_{in}|^4 + \kappa_p^6)]|\alpha_{in}|^2$. Therefore, the first-order and second-order approximations of the transmission can be written as

$$T^{(1)} \approx \frac{4\kappa_{p,e}^2\kappa_p^4}{16\eta^2\kappa_{p,e}^2|\alpha_{in}|^4 + \kappa_p^6}, \quad (13a)$$

$$T^{(2)} \approx \frac{4\kappa_{p,e}^2}{4\eta^2\langle\hat{c}^\dagger\hat{c}\rangle_2^2 + \kappa_p^2}. \quad (13b)$$

C. Vacuum-induced bound state of phonons

The WQR system for the SAW phonon blockade is shown in Fig. 2(a). Instead of coupling to the SAW resonator, the qubit couples to a SAW mode with a coupling constant V , which propagates at a velocity v_g in the one-dimensional (1D) SAW waveguide. This coupling causes the qubit to decay at a rate of $\Gamma = V^2/v_g$ to the waveguide. Similarly, the qubit simultaneously couples to a MW resonator with resonance frequency ω_m and the coupling strength is g_m . It decays to the environment with an intrinsic rate γ . We consider a weak SAW pulse with a narrow bandwidth propagating in the 1D SAW waveguide and that the qubit couples to the MW resonator mode much stronger than the SAW waveguide mode. Note that the propagating SAW pulse is coherently generated by electrical signals via the interdigital transducer [20,28,79–81]. Because it is mature to control the temporal duration and the shape of an electric signal, the spectrum of a SAW pulse can be narrow and well controlled [79]. Recently, it has been experimentally demonstrated that a propagating SAW pulse with MHz-level bandwidth couples to a two-level transmon qubit [28,81]. In this WQR system, we take the phononic bandwidth and the couplings to the SAW and quantum vacuum field to be much smaller than the anharmonicity to ensure that the state $|e\rangle$ is barely excited. Thus, the second excited state $|f\rangle$ can be excluded in the model [81–83]. In this arrangement, we can treat the qubit as a two-level system, and truncate the MW resonator up to the Fock state $|1_m\rangle$. The qubit-MW-resonator subsystem can be modeled as a four-level system with $|1\rangle = |g, 0_m\rangle$ for the vacuum state, $|2\rangle = |e, 0_m\rangle$, $|3\rangle = |g, 1_m\rangle$, and $|4\rangle = |e, 1_m\rangle$ [74] [see Fig. 2(b)].

Considering a linear dispersion of the waveguide at ω_{in} , we have the Hamiltonian describing a moving SAW pulse coupling to the WQR system as [84–86]

$$\begin{aligned} \hat{H}_{\text{WQR}} = & -i \int dx v_g \left[\hat{c}_R^\dagger(x) \frac{d}{dx} \hat{c}_R(x) - \hat{c}_L^\dagger(x) \frac{d}{dx} \hat{c}_L(x) \right] \\ & + \int dx V \delta(x) [\hat{\sigma}^+ \hat{c}_R(x) + \hat{c}_R^\dagger(x) \hat{\sigma}^- \\ & + \hat{\sigma}^+ \hat{c}_L(x) + \hat{c}_L^\dagger(x) \hat{\sigma}^-] \\ & + (\bar{\Delta}_m - i\kappa_m) \hat{a}^\dagger \hat{a} + (\bar{\Delta}_q - i\gamma) \hat{\sigma}_{ee} \\ & + g_m (\hat{a}^\dagger \hat{\sigma}^- + \hat{\sigma}^+ \hat{a}), \end{aligned} \quad (14)$$

where $\hat{c}_{R,L}^\dagger(x)$ are the creation operators for the right-moving (left-moving) phonons at x , $\bar{\Delta}_m = \omega_m - \omega_{in}$, and $\bar{\Delta}_q = \omega_e - \omega_{in}$.

In the N-type picture, the Hamiltonian \hat{H}_{WQR} reads

$$\begin{aligned} \hat{H}'_{\text{WQR}} = & -i \int dx v_g \left[\hat{c}_R^\dagger(x) \frac{d}{dx} \hat{c}_R(x) - \hat{c}_L^\dagger(x) \frac{d}{dx} \hat{c}_L(x) \right] \\ & + (\bar{\Delta}_q - i\gamma) \hat{S}_{22} + (\bar{\Delta}_m - i\kappa_m) \hat{S}_{33} \\ & + (\Delta_4 - i\kappa_m - i\gamma) \hat{S}_{44} \\ & + \int dx V \delta(x) \{ [\hat{c}_R^\dagger(x) + \hat{c}_L^\dagger(x)] (\hat{S}_{12} + \hat{S}_{34}) + \text{H.c.} \} \\ & + g_m (\hat{S}_{23} + \hat{S}_{32}), \end{aligned} \quad (15)$$

with $\Delta_4 = (\bar{\Delta}_m + \bar{\Delta}_q)$. In this model, a phonon mode propagating in the 1D waveguide drives the transitions of $|1\rangle \leftrightarrow |2\rangle$ and $|3\rangle \leftrightarrow |4\rangle$. The excited states $|2\rangle$, $|3\rangle$, and $|4\rangle$ decay at the rates of γ , κ_m , and $\kappa_m + \gamma$, respectively.

Typically, an N-type atom coupling to a 1D photonic waveguide generates photon-photon bound states with the help of a coherent control field and thus results in photon blockade [68,87]. Here, we show that a phonon-phonon bound state can also be created by a MW quantum vacuum field, yielding blockade of propagating SAW phonons. In our protocol, the MW quantum vacuum field, coupling to the qubit with a rate g_m , plays the role of the external control field in the previous protocol [87]. Following Refs. [68,85,87–89], the scattering eigenstates can be constructed explicitly by imposing an open boundary condition and setting that the incident phonon state be a freely moving SAW.

After converting the right- and left-moving modes to the odd-even mode basis, we can conveniently solve the eigenstates of one-phonon and two-phonon scattering, and get the corresponding scattering matrices for deriving the output state $|\psi\rangle$ (see Appendix B). For a weak incident SAW, the second-order correlation function $g^{(2)}(0)$ of the transmission mode [87], considering the contribution of both one- and two-phonon states, is given by

$$g^{(2)}(0) = \frac{|\int dk_1 dk_2 \alpha(k_1) \alpha(k_2) (t_{k_1} t_{k_2} - r_{k_1} r_{k_2})|^2}{|\int dk_1 dk_2 \alpha(k_1) \alpha(k_2) t_{k_1} t_{k_2}|^2}, \quad (16)$$

where $t_{k_{1,2}}$ and $r_{k_{1,2}}$ correspond to single-phonon transmission and reflection coefficients, respectively. In the numerator, the first term comes from the plane wave (PW), and the second one from the bound state (BS), as in [87] (see Appendix B).

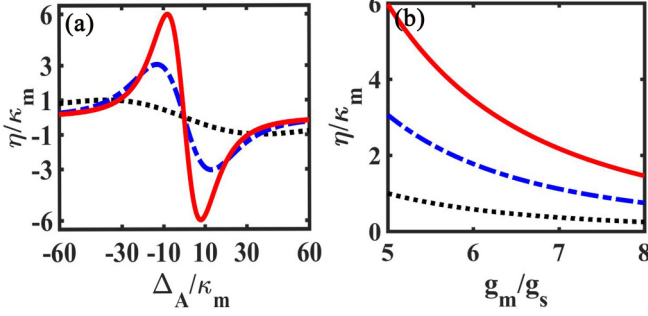


FIG. 3. (a) Kerr nonlinearity η versus Δ_A with $g_m/g_s = 5$, $g_s/\kappa_m = 10$. (b) Kerr nonlinearity η versus g_m/g_s . When scanning Δ_A , we take the value of Δ_A at the point where η is at its maximum. The solid red (dashed blue, dotted black) curve is calculated with $\Delta_M/\Delta_A = 11.4$ (4.20, 1.36) and $\gamma/\kappa_m = 0.05$ both in (a) and (b).

To show the effect of the microwave vacuum field, we take the single-phonon transmission as an example. According to the scattering state $|\psi^{(1)}\rangle$ in Eq. (B10a), the transmission T for the one-phonon state can be written as

$$\begin{aligned} T &= \int_{k>0} dk |k|\psi^{(1)}|^2 \\ &= \int_{k>0} dk \alpha^2(k) |t_k|^2. \end{aligned} \quad (17)$$

III. RESULTS

In the following investigation, we consider an experimental available qubit anharmonicity of $\alpha \sim 2\pi \times 250$ MHz and a typical value of $\kappa_m \sim 2\pi \times 1$ MHz [10,17,26].

A. Self-Kerr-nonlinearity-induced SAW phonon blockade

Below we first numerically calculate the self-Kerr nonlinearity in our RQR system (see Fig. 3), and then present evidences for the phonon blockade, indicated by $g^{(2)}(0) < 0.5$ in Fig. 4, with experimental accessible parameters. In Fig. 3(a), we take $g_m = 5g_s$, that $\langle \hat{\rho}_{11} \rangle \approx 1$. The self-Kerr

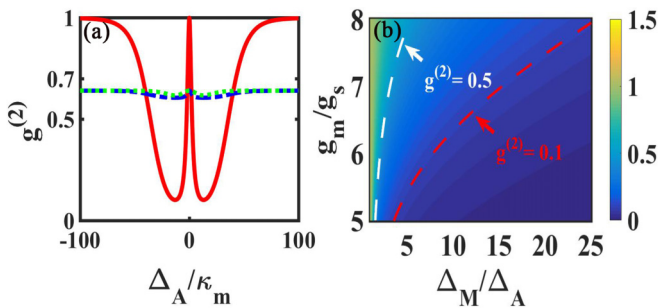


FIG. 4. (a) The second-order correlation $g^{(2)}(0)$ (the solid red curve) and the transmission (dashed blue and dotted green curves) as a function of Δ_A , where the dashed blue curve is the result of numerical simulation, and the dotted green curve is the analytic result approximating to the first order. (b) $g^{(2)}(0)$ as a function of g_m/g_s and Δ_M/Δ_A . When scanning Δ_A , we take the value of Δ_A at the point where η is at its maximum. $\Gamma_\phi = 0$, $\gamma/\kappa_m = 0.05$, $\kappa_{p,i}/\kappa_m = 0.2$, and $\kappa_{p,e1} = \kappa_{p,e2} = 2\kappa_{p,i}$ in both (a) and (b), and $g_m/g_s = 5$ in (a).

nonlinearity η has a “dispersive” profile and is zero at $\Delta_A = 0$. When $\Delta_M/\Delta_A = 1.36$, the maximal absolute value $|\eta|$ is close to κ_m in the region $|\Delta_A|/\kappa_m > 30$. It increases to $3\kappa_m$ at $\Delta_A = \pm 13\kappa_m$ for $\Delta_M/\Delta_A = 4.20$. For a larger ratio Δ_M/Δ_A , e.g., $\Delta_M/\Delta_A = 11.4$, the Kerr nonlinearity $|\eta|$ reaches a peak value $6\kappa_m$ at about $\Delta_A = \pm 8\kappa_m$, much larger than the decay rate κ_p of the SAW resonator; here we take $\kappa_p \approx \kappa_m$. Using these values for parameters of our system, the SAW and the MW field decouple from the transition between $|e\rangle$ and $|f\rangle$. The qubit can be treated as a two-level system. The nonlinearity $|\eta|$ becomes larger as Δ_M/Δ_A increases. Furthermore, the available strongest nonlinearity decreases as g_m/g_s increases [see Fig. 3(b)]. The results above are well understood and inconsistent with the approximate formulas in Sec. II [see Eq. (6)].

Here, we present an intuitive picture to explain these trends. In our system, we use the self-Kerr nonlinear modulation to implement the phonon blockade. From the energy level diagram in Fig. 1(b), we can see that, to create a strong phononic nonlinearity, the phonon needs to drive the transitions of $1 \leftrightarrow 2$ and $3 \leftrightarrow 4$ simultaneously. However, if a very large coupling rate g_m is applied, the population of $\hat{\rho}_{33}$ will be negligibly small, and thus the transition of $3 \leftrightarrow 4$ will become null and have no contribution. As a result, the N-type energy level will reduce to a three-level Λ -type system. This eventually significantly suppresses the self-Kerr nonlinearity. On the contrary, with the decrease of g_m/g_s and the increase of Δ_M/Δ_A , the system has a greater probability of excitation to the higher energy levels $|2\rangle$, $|3\rangle$, and $|4\rangle$ [57]. In this sense, a larger self-Kerr nonlinearity can be obtained. On the other hand, the perturbation analysis method requires the assumption of $\rho_{11} \approx 1$, i.e., most of the population of atoms in the ground state $|1\rangle$. Thus, there is a competition between making the perturbation approach effective and getting a large nonlinearity. Measuring this competitive relationship is difficult, and we will make a qualitative analysis of this relationship in the following paragraph. In practice, we can obtain $\eta > 3\kappa_m$ for a large ratio $g_m/g_s > 5$, yielding $\langle \hat{\rho}_{11} \rangle \approx 1$, by choosing a proper value of Δ_M/Δ_A . This large self-Kerr nonlinearity allows us to achieve a strong phonon blockade.

Phonon blockade can be identified with the second-order correlation function $g^{(2)}(0)$ as shown in Fig. 4. To eliminate the influence of the unwanted linear shift term, we choose $\bar{\Delta} = \Delta_a$, which can be achieved by adjusting the probe frequency ω_{in} . We evaluate the performance of the phonon blockade by using the experimental available values $\kappa_{p,i} = 0.2\kappa_m$ and $\kappa_{p,e1} = \kappa_{p,e2} = 2\kappa_{p,i}$ [15,17,29,30,90]. As expected, the dips of $g^{(2)}(0)$ appear where the nonlinearity is the strongest value for given parameters, as shown in Fig. 4(a). For $\eta = 3\kappa_m$, the second-order correlation function (red solid curve) is small, $g^{(2)}(0) < 0.1$, at $\Delta_A = \pm 13\kappa_m$. Phonon blockade disappears in the vicinity of $\Delta_A = 0$ because the Kerr nonlinearity is weak. In Fig. 4(b), $g^{(2)}(0)$ is shown as a function of g_m/g_s and Δ_M/Δ_A . We find that, to achieve the phonon blockade, the ratio Δ_M/Δ_A needs to be larger as the ratio g_m/g_s increases. If Δ_M/Δ_A is not large enough, one can only obtain a weak phonon blockade, as indicated by the white curve for $g^{(2)}(0) = 0.5$. In contrast, we can achieve $g^{(2)}(0) < 0.1$, corresponding to a deep phonon blockade, when Δ_M is very different from Δ_A .

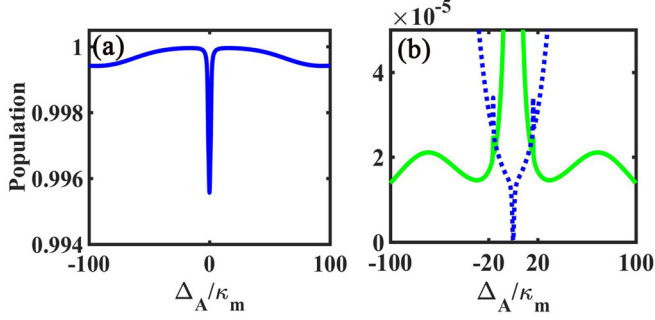


FIG. 5. The steady-state excitation of the state $|1\rangle$ (a) and the MW resonator and the qubit as a function of Δ_A . $\gamma/\kappa_m = 0.05$, $\kappa_{p,i}/\kappa_m = 0.2$, $\kappa_{p,e1} = \kappa_{p,e2} = 2\kappa_{p,i}$, $g_s/\kappa_m = 10$, $g_m = 5g_s$, $\alpha_{in}/\sqrt{\kappa_m} = 0.2$, and $\Delta_M/\Delta_A = 4.2$. In (b), the solid green curve is for the MW resonator, and the dashed blue curve for the qubit.

Equation (3) and the subsequent numerical simulations are valid only on the basis of the perturbation approach [36,60,75–77]. This approach requires $g_s \ll g_m$ and a weak SAW probe so that the zero-photon state in the MW resonator is mostly occupied, i.e., $\hat{\rho}_{11} \approx 1$. In deriving the self-Kerr nonlinearity, we ignore some terms that are proportional to g_s , which are smaller than the g_m terms (see Appendix A). However, this condition reduces the nonlinearity and weakens the effect of the phonon blockade according to Eq. (3) and the above analysis. In our system, we have the controllable detunings Δ_M and Δ_A , and we can compensate for the loss of nonlinearity when we want the system to satisfy the perturbation method.

To proof our assumption of $\langle \hat{\rho}_{11} \rangle \approx 1$, the steady-state population of $\langle \hat{\rho}_{11} \rangle$ and the excited MW photon in the MW resonator are shown in Fig. 5. Clearly, the N-type system is mainly in the state $|1\rangle = |g, 0_m\rangle$ and satisfies the assumption $\langle \hat{\rho}_{11} \rangle \approx 1$. Meanwhile, the MW resonator is mostly in its quantum vacuum state, since the mean number of MW photons is about 10^{-5} , shown in Fig. 5(b).

It is important to achieve the high transmission with a small $g^{(2)}(0)$ for quantum information processing, but this target is usually challenging [43,91]. In contrast, our system can achieve a small $g^{(2)}(0) = 0.1$ and a high transmission of about 0.6 [see the dashed blue curve in the numerical simulation and the dotted green curve in the analytical result to approximate the first order in Fig. 4(a)].

From Eq. (11), we can find that, the transmission returns to its standard form $T_s = (2\kappa_{p,e})^2/\kappa_p^2$ in the absence of self-Kerr nonlinearity, i.e., $\eta = 0$. At this time, the transmission can approach one, when $\kappa_{p,e} \gg \kappa_{p,i}$. When $\eta > \kappa_m$, the transmission decreases and the phonon blockade prevents the transmission of high phonon states, due to a strong self-Kerr nonlinearity. Numerical and analytical results are in quantitative agreement as shown in Fig. 6. When $\eta = 3\kappa_m$, the phonon self-Kerr nonlinearity can lead to the phonon blockade and subsequently a small $g^{(2)}(0) = 0.1$ at $\Delta_A \approx \pm 13\kappa_m$ [see Fig. 4(a)]. At the same time, the transmission is 0.605 [see Fig. 6(a) (solid red curve)]. This value is in good agreement with the analytical results calculated from the first- and the second-order approximations within a range where the absolute value of Δ_A/κ_m is small (blue dashed and green dotted curves). However,

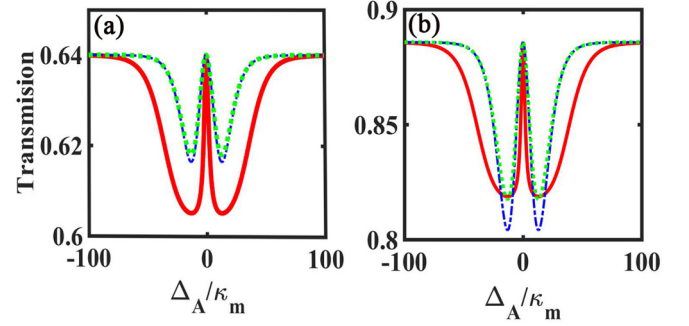


FIG. 6. Transmission of the RQR system as a function of the detuning Δ_A/κ_m . (a) Transmission for the SAW resonator with $\kappa_{p,i}/\kappa_m = 0.2$, $\kappa_{p,e1} = \kappa_{p,e2} = 2\kappa_{p,i}$. (b) Transmission for the SAW resonator with $\kappa_{p,i}/\kappa_m = 0.05$, $\kappa_{p,e1} = \kappa_{p,e2} = 8\kappa_{p,i}$. Both in (a) and (b), $\gamma/\kappa_m = 0.05$, $g_s/\kappa_m = 10$, $g_m/g_s = 5$, $\alpha_{in}/\sqrt{\kappa_m} = 0.2$, $\Delta_M/\Delta_A = 4.2$, $\eta/\kappa_m = 3$, and $\bar{\Delta} = \Delta_a$, yielding a zero effective detuning. The solid red curve is the result of numerical simulation, and the blue dashed and green dotted curves are the analytical results approximating the first and second order.

when the absolute value of Δ_A/κ_m is relatively large, η/κ_m will become larger (see Fig. 3), and then the assumption of $2\eta\langle \hat{c}^\dagger \hat{c} \rangle_0 \ll \kappa_p$ used in our model calculation will become weaker. Therefore, the numerical and analytical results will be slightly different. When the external coupling is stronger, e.g., $\kappa_{p,i}/\kappa_m = 0.05$ [17], a higher transmission with $T = 0.82$ is achieved at $\Delta_A \approx \pm 13\kappa_m$ [see Fig. 6(b)]. It can also be clearly seen that the second-order approximation including more precise correction fits the numerical result better than the first-order one. Thus, improving the ratio $\kappa_{p,e}/\kappa_{p,i}$ can lead to a larger transmission, which is limited by $T_s = (2\kappa_{p,e})^2/\kappa_p^2$.

We also analyze the effects of η and α_{in} on the transmission as shown in Fig. 7. As expected, the transmission T decreases when the self-Kerr nonlinear interaction strength η increases. For a weak probe with $\alpha_{in} \lesssim 0.3\sqrt{\kappa_m}$, the population of high phonon states is small, and the phonon resonator is weakly excited, i.e., $\langle \hat{c}^\dagger \hat{c} \rangle \sim 0$. In this regime, the transmission T is relatively large and the analytical results are in good agree-

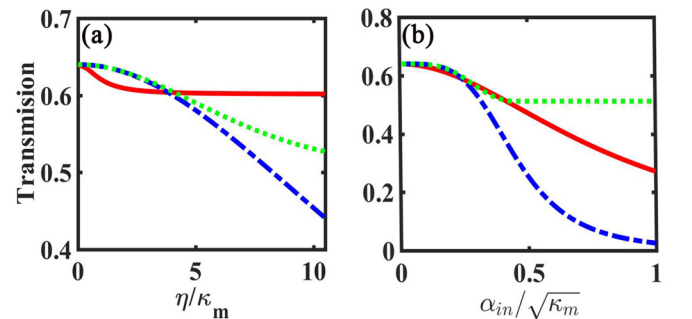


FIG. 7. (a) Transmission of the RQR system versus self-Kerr nonlinearity η with $\alpha_{in}/\sqrt{\kappa_m} = 0.2$. (b) Transmission of the RQR system versus α_{in} with $\Delta_M/\Delta_A = 4.2$. Here $\gamma/\kappa_m = 0.05$, $\kappa_{p,i}/\kappa_m = 0.2$, $\kappa_{p,e1} = \kappa_{p,e2} = 2\kappa_{p,i}$, $g_s/\kappa_m = 10$, $g_m/g_s = 5$. The solid red curve is the result of numerical simulation, and the blue dashed and green dotted curves are the analytical results approximating the first and second order.

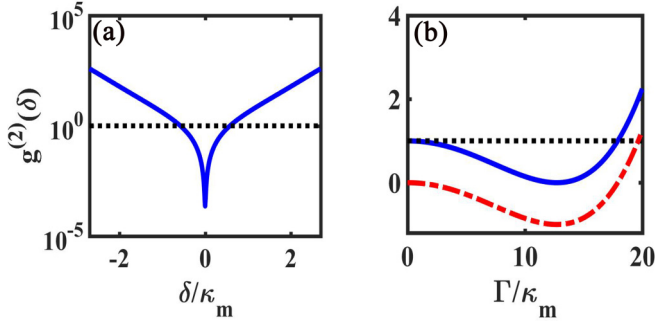


FIG. 8. (a) The second-order correlation $g^{(2)}(0)$ (blue solid curve) versus the detuning $\delta = \omega_{\text{in}} - \bar{\Delta}_q$. The black dotted line is for $g^{(2)}(0) = 1$. Taking $\gamma = \kappa_m$, $\Delta_M = 0$, $g_m = 3.5\kappa_m$, $\Gamma = 12.8\kappa_m$, and $\sigma = 0.2\kappa_m$. (b) $g^{(2)}(0)$ (blue curve), the PW contribution (black dotted line) and the BS contribution (red dotted-dashed curve) as a function of waveguide caused decay Γ . Setting $\delta = 0$, other parameters are the same as in (a).

ment with the numerical calculation. As α_{in} increases, the first term of the denominator of Eq. (11), including α_{in} , becomes larger and thus leads to a smaller transmission. Note that the analytical results are based on the iteration method, which no longer applies when $\langle \hat{c}^\dagger \hat{c} \rangle$ and η is large.

B. Bound-state-induced SAW phonon blockade

Now we show the vacuum-induced bound states of a SAW and the resulting phonon blockade in the 1D SAW waveguide. We consider a Gaussian SAW wave function $\alpha(k) = (1/(2\pi\sigma^2)^{1/4}) \exp(-(k - k_0)^2/(4\sigma^2))$ for the input, where σ is the bandwidth, and $k_0 = \omega_{\text{in}}$ ($v_g = 1$ for simplicity). In calculation, we take $\kappa_m = \gamma$, $\Delta_M = 0$, $g_m = 3.5\kappa_m$, $\Gamma = 12.8\kappa_m$, and $\sigma = 0.2\kappa_m \sim 2\pi \times 0.2$ MHz. Experiments have demonstrated the generation of SAW pulses with such narrow bandwidth [20,79–81]. Thus, the bandwidth of the SAW phonon pulse and the SAW-qubit coupling are much smaller than the anharmonicity of the qubit, avoiding the driving to the state $|f\rangle$. Without the BS contribution, the transmitted phonon shows a trivial Poissonian distribution and $g^{(2)}(0) = 1$ [black dotted lines in Fig. 8(b)]. When the BS part is taken into account, we obtain the phonon blockade, i.e., $g^{(2)}(0) < 0.5$, in the region of $|\delta| < 0.43\kappa_m$ [see blue curve in Fig. 8(a)]. When the PW and BS contributions are out of phase, the quantum destructive interference between the plan wave and the bound state parts can lead to the phonon blockade, as shown by blue solid and red dotted-dashed curves in Fig. 8(b). When Γ is small, indicating a weak waveguide-qubit coupling, the BS contribution is negligible. Thus, the phonon blockade is not achievable as the case without the BS contribution. As Γ increases, the BS contribution becomes larger. When the BS component cancels out the PW contribution, the phonon statistics is antibunching that $g^{(2)}(0) < 1$. As Γ increases further, the BS contribution overwhelms the PW part, resulting in $g^{(2)}(0) > 1$ again. As our analysis in Sec. II B, the phonon bound state is induced by the N-type system resulting from the vacuum-qubit coupling. Therefore, we clearly show the vacuum-induced phonon blockade in a traveling SAW field.

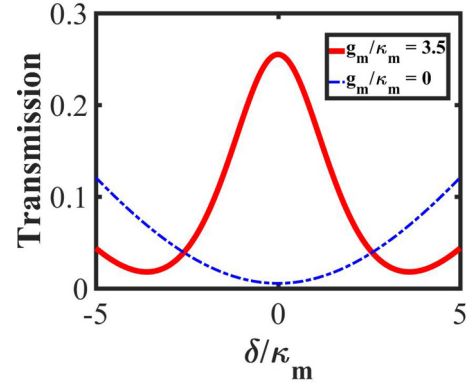


FIG. 9. The transmission of one phonon as a function of $\delta = \omega_{\text{in}} - \bar{\Delta}_q$ for $g_m/\kappa_m = 3.5$ (solid red curve) and $g_m/\kappa_m = 0$ (dashed-dotted blue curve). Other parameters take values $\kappa_m = \gamma$, $\Delta_M = 0$, $\Gamma/\kappa_m = 12.8$, $\sigma/\kappa_m = 0.2$.

High transmission is important in creating a Fock state via blockade but normally difficult. Here, we show a relatively high transmission in the phonon blockade using our WQR configuration. As shown in Fig. 9, without the MW resonator, i.e., $g_m = 0$, the transmission is zero at $\delta = 0$ (dashed-dotted blue curve). The single SAW phonon wave packet is reflected by the qubit [68]. When the qubit strongly couples to the MW resonator, e.g., $g_m/\kappa_m = 3.5$, and the transmission significantly increases and reaches 0.25 near resonance ($\delta/\kappa_m \sim 0$) (see the red curve in Fig. 9). This is similar to the vacuum-induced-transparent phenomenon in the optical regime, and in principle enables MW-photon-number-dependent quantum devices [66].

IV. IMPLEMENTATION

The schematic design of our protocol is depicted in Fig. 1. It involves a superconducting qubit coupling to a SAW resonator or waveguide and a MW resonator. The SAW probe can be input into and lead out the system via IDTs. The required experimental technology has been developed recently [17,20,28]. The key requirement of our system is the strong coupling of the transmon qubit to a SAW resonator or a 1D SAW waveguide. Using the existing experimental technique, a transmon qubit can couple to a SAW resonator [17,28] or a waveguide [20] via the IDT made on a AlN or LiNbO₃ film. The coupling strength can be further enhanced by applying a larger IDT with more fingers or focusing the SAW to a smaller region with a curved IDT [92,93]. The coupling strength varies from a few to tens of MHz using AlN [17,20] and can be even stronger using LiNbO₃ due to the larger Pockels coefficient. The decay rate of a transmon qubit recently reduces to a few kHz [10], and its pure dephasing Γ_ϕ is negligible. The MW-qubit coupling can reach $2\pi \times 100$ MHz, e.g., $g_m/2\pi \sim 60$ MHz [17], or even to GHz [94]. A MW resonator normally decays at a rate of about $\kappa_m/2\pi \sim 1$ MHz [17]. The decay rate of the SAW resonator is much smaller, e.g., $\kappa_{p,i}/2\pi = 36$ kHz [17]. In the estimate of the performance of the phonon blockade, we consider a superconducting qubit with an anharmonicity $\alpha \sim 2\pi \times 250$ MHz, which can be treated as a two-level system

well. We also take experimentally available values for parameters that $\kappa_m/2\pi = 1$ MHz, $g_m/2\pi = 50$ MHz, $\gamma/2\pi = 50$ kHz. When $g_s/2\pi = 10$ MHz, $\Delta_M/2\pi = 91.2$ MHz, and $\Delta_A/2\pi = 8$ MHz that $\Delta_M = 11.4\Delta_A$ in the RQR system, and obtain $g^{(2)}(0) = 0.029$, indicating a deep phonon blockade. In the WQR system, we take $\Gamma/2\pi = 12.8$ MHz, $\Delta_M = 0$, and $g_m = 3.5$ MHz and consider a weak SAW pulse with bandwidth $\sigma = 2\pi \times 0.2$ MHz, and we have $g^{(2)}(0) < 0.5$ for $|\delta| < 0.43\kappa_m$.

V. DISCUSSION AND CONCLUSION

The vacuum-induced effects have been observed in several experiments recently [63,65,66]. Controlling or manipulation of a quantum system via the quantum vacuum field can be essentially different from a classical coherent control version. In our systems, the transition $2 \leftrightarrow 3$ is driven by the MW quantum vacuum field with a rate g_m . It is worthy of noting that the photon number variance, $\langle \hat{a}^\dagger \hat{a} \rangle = \langle (\hat{a}^\dagger \hat{a})^2 \rangle - \langle \hat{a}^\dagger \hat{a} \rangle^2$, of the quantum vacuum field is zero. Therefore, we can obtain a shot-noise-free self-Kerr phononic nonlinearity as given by Eq. (3). However, in the classical version, the classical coherent field $|\alpha\rangle$ has a quantum uncertainty proportional to α [77,95–97]. This intensity-dependent uncertainty can cause fluctuation in the controlled quantum system. In previous conventional schemes creating the giant photonic self-Kerr nonlinearity with an N-type system, a coherent control field $|\alpha\rangle$ is applied. The vacuum-field-qubit coupling g_m need to be replaced by $g_c = g'_m \sqrt{\hat{N}_c}$, where \hat{N}_c is the phonon number operator of the coherent field $|\alpha\rangle$ and g'_m is the average single-photon coupling rate. As in Eq. (3), the induced self-Kerr nonlinearity is crucially dependent on the intensity of the control field. As a result, the phonon number uncertainty, $\propto \sqrt{\hat{N}_c}$, of the coherent control field inevitably causes fluctuation of the self-Kerr nonlinearity and subsequently in the photon blockade. Therefore, our vacuum-field-control version has potential advantages over the conventional coherent-field scheme. But a detailed discussion and numerical simulation are beyond the topic of this paper. We will address this point in the future work.

In conclusion, we have proposed an N-type quantum system for SAW phonon blockade with simultaneously achieving high transmission. By coupling this system to a SAW resonator, we have created a large self-Kerr phononic nonlinearity and shown the phonon blockade. When this N-type system couples to a propagating SAW via a 1D SAW waveguide, it creates a bound state and also leads to blockade of transmitted phonons moving in the waveguide. Interestingly, the phonon blockade is induced by the vacuum-qubit coupling. Our proposal may pave the way for SAW-phonon-based quantum information processing in SQC platform. We note that a Λ -type atom can be transparent to a freely propagating weak probe light when its states are strongly dressed by a cavity vacuum field, leading to the vacuum-induced transparency (VIT) [66]. Our vacuum-induced phonon blockade studies the quantum statistics of transmitted SAW phonons through a resonator and thus is essentially different from VIT.

ACKNOWLEDGMENTS

H.Z., K.X., M.X., and Y.L. thank the support of the National Key R&D Program of China (Grants No. 2017YFA0303703, No. 2017YFA0303701, No. 2019YFA0308700, and No. 2019YFA0308704). This work is also supported by the National Natural Science Foundation of China (Grants No. 11874212, No. 11890704, No. 61671279, No. 11574145, No. 11690031, and No. 11904171), and the Natural Science Foundation of Jiangsu Province (Grant No. BK20180461).

APPENDIX A: THE EFFECTIVE SELF-KERR NONLINEAR COEFFICIENT

In this subsection, we derive the effective self-Kerr nonlinear coefficient using the perturbation approach [60,75–77]. The RQR system consists of a microwave (MW) resonator, a superconducting transmon qubit, and a SAW resonator [see Fig. 1(a) in the main text]. The qubit is treated as a two-level system with the ground and excited states, $|g\rangle$ and $|e\rangle$, respectively. The resonance frequencies, ω_A , ω_e , and ω_m , of the SAW resonator, the qubit, and the MW resonator are about a few GHz.

For the RQR system without the probe, the Hamiltonian can be written as ($\hbar = 1$)

$$\begin{aligned} \tilde{H}_{\text{RQR}} = & \omega_A \hat{c}^\dagger \hat{c} + \omega_m \hat{a}^\dagger \hat{a} + \omega_e \hat{\sigma}_{ee} + g_s (\hat{c}^\dagger \hat{\sigma}_{ge} + \hat{\sigma}_{eg} \hat{c}) \\ & + g_m (\hat{a}^\dagger \hat{\sigma}_{ge} + \hat{\sigma}_{eg} \hat{a}), \end{aligned} \quad (\text{A1})$$

\hat{c} (\hat{a}) is the annihilation operator of the SAW (MW) resonator, and $\hat{\sigma}_{kl} \equiv |k\rangle\langle l|$ ($k, l = g, e$). g_s and g_m are the coupling strengths. In the rotating frame, defined by the unitary transformation as

$$\tilde{U}_1 = \exp\{i[\omega_A \hat{c}^\dagger \hat{c} + \omega_A \hat{a}^\dagger \hat{a} + \omega_A \hat{\sigma}_{ee}]t\}, \quad (\text{A2})$$

the Hamiltonian in the interaction picture takes the form,

$$\begin{aligned} \hat{H}_{\text{RQR}} = & (\Delta_M - \Delta_A) \hat{a}^\dagger \hat{a} - \Delta_A \hat{\sigma}_{ee} + g_m (\hat{a}^\dagger \hat{\sigma}_{ge} + \hat{\sigma}_{eg} \hat{a}) \\ & + g_s (\hat{c}^\dagger \hat{\sigma}_{ge} + \hat{\sigma}_{eg} \hat{c}), \end{aligned} \quad (\text{A3})$$

where $\Delta_A = \omega_A - \omega_e$ ($\Delta_M = \omega_m - \omega_e$) denotes the detuning between the SAW resonator (the MW resonator) and the qubit. The third (fourth) describes the interaction of the qubit and the MW (SAW) resonator.

At cryogenic temperature, e.g., 20 mK, the thermal excitation of the MW resonator is negligible. The MW resonator is mostly populated in the vacuum state $|0_m\rangle$. The qubit is also in its ground state without external driving. We consider the situation that the qubit-MW interaction is much stronger than the coupling of the qubit to the SAW phonon resonator. In this case, the qubit and the MW resonator mostly stays in the state $|g, 0_m\rangle$. We can truncate the MW resonator up to the Fock state $|1_m\rangle$, and obtain an N-type four-level system (4LS) modeling the RQR system, shown in Fig. 1(b). The four states of the N-type configuration are denoted as $|1\rangle = |g, 0_m\rangle$, $|2\rangle = |e, 0_m\rangle$, $|3\rangle = |g, 1_m\rangle$, and $|4\rangle = |e, 1_m\rangle$. The SAW phonon drives the transitions of $|1\rangle \leftrightarrow |2\rangle$ and $|3\rangle \leftrightarrow |4\rangle$. Here, the typically coherent control driving in the photonic counterpart is replaced by the quantum vacuum-field-qubit coupling g_m . This N-type

system is used to create a giant self-Kerr nonlinearity in the SAW phonon resonator.

In the basis of $\{|1\rangle, |2\rangle, |3\rangle, |4\rangle\}$, the Hamiltonian \hat{H}_{RQR} in Eq. (A3) becomes

$$\begin{aligned} \hat{H}'_{\text{RQR}} = & (\Delta_M - \Delta_A)(\hat{S}_{33} + \hat{S}_{44}) - \Delta_A(\hat{S}_{22} + \hat{S}_{44}) \\ & + (g_m \hat{S}_{32} + g_s \hat{c}^\dagger \hat{S}_{12} + g_s \hat{c}^\dagger \hat{S}_{34} + \text{H.c.}), \end{aligned} \quad (\text{A4})$$

where $\hat{S}_{mn} = |m\rangle\langle n|$ ($m, n = 1, 2, 3, 4$). The decay and dephasing of the system can be described by the Lindblad operator:

$$\begin{aligned} \mathcal{L}\hat{Q} = & \frac{\kappa_m}{2} \{2\hat{a}^\dagger \hat{Q} \hat{a} - \hat{a}^\dagger \hat{a} \hat{Q} - \hat{Q} \hat{a}^\dagger \hat{a}\} \\ & + \frac{\gamma}{2} \{2\hat{\sigma}^+ \hat{Q} \hat{\sigma}^- - \hat{\sigma}^+ \hat{\sigma}^- \hat{Q} - \hat{Q} \hat{\sigma}^+ \hat{\sigma}^-\} \\ & + \frac{\Gamma_\phi}{2} \{2\hat{\sigma}_{ee} \hat{Q} \hat{\sigma}_{ee} - \hat{\sigma}_{ee} \hat{Q} - \hat{Q} \hat{\sigma}_{ee}\}, \end{aligned} \quad (\text{A5})$$

where κ_m and γ are the decay rates of the microwave resonator and the qubit, respectively. Γ_ϕ represents the dephasing of the excited state of the qubit. Then, the Heisenberg's equations for the system take the form,

$$\dot{\hat{S}}_{11} = ig_s(\hat{S}_{21}\hat{c} - \hat{c}^\dagger \hat{S}_{12}) + \kappa_m \hat{S}_{33} + \gamma \hat{S}_{22}, \quad (\text{A6a})$$

$$\dot{\hat{S}}_{22} = ig_m(\hat{S}_{32} - \hat{S}_{23}) + ig_s(\hat{c}^\dagger \hat{S}_{12} - \hat{S}_{21}\hat{c}) + \kappa_m \hat{S}_{44} - \gamma \hat{S}_{22}, \quad (\text{A6b})$$

$$\dot{\hat{S}}_{33} = ig_m(\hat{S}_{23} - \hat{S}_{32}) + ig_s(\hat{S}_{43}\hat{c} - \hat{c}^\dagger \hat{S}_{34}) - \kappa_m \hat{S}_{33} + \gamma \hat{S}_{44}, \quad (\text{A6c})$$

$$\dot{\hat{S}}_{44} = ig_s(\hat{c}^\dagger \hat{S}_{34} - \hat{S}_{43}\hat{c}) - (\kappa_m + \gamma) \hat{S}_{44}, \quad (\text{A6d})$$

$$\begin{aligned} \dot{\hat{S}}_{21} = & ig_m \hat{S}_{31} + ig_s \hat{c}^\dagger (\hat{S}_{11} - \hat{S}_{22}) - i\Delta_A \hat{S}_{21} \\ & + \kappa_m \hat{S}_{43} - \left(\frac{\gamma}{2} + \frac{\Gamma_\phi}{2}\right) \hat{S}_{21}, \end{aligned} \quad (\text{A6e})$$

$$\begin{aligned} \dot{\hat{S}}_{23} = & ig_m(\hat{S}_{33} - \hat{S}_{22}) + ig_s \hat{c}^\dagger (\hat{S}_{13} - \hat{S}_{24}) \\ & - \left(i\Delta_M + \frac{\kappa_m}{2} + \frac{\gamma}{2} + \frac{\Gamma_\phi}{2}\right) \hat{S}_{23}, \end{aligned} \quad (\text{A6f})$$

$$\begin{aligned} \dot{\hat{S}}_{43} = & \left(-i\Delta_A - \kappa_m - \frac{\gamma}{2} - \frac{\Gamma_\phi}{2}\right) \hat{S}_{43} + ig_s \hat{c}^\dagger (\hat{S}_{33} - \hat{S}_{44}) \\ & - ig_m \hat{S}_{42}, \end{aligned} \quad (\text{A6g})$$

$$\begin{aligned} \dot{\hat{S}}_{31} = & ig_m \hat{S}_{21} + ig_s \hat{S}_{41} \hat{c} - ig_s \hat{c}^\dagger \hat{S}_{32} \\ & + \left[i(\Delta_M - \Delta_A) - \frac{\kappa_m}{2}\right] \hat{S}_{31} + \gamma \hat{S}_{42}, \end{aligned} \quad (\text{A6h})$$

$$\begin{aligned} \dot{\hat{S}}_{41} = & ig_s \hat{c}^\dagger \hat{S}_{31} - ig_s \hat{c}^\dagger \hat{S}_{42} \\ & + \left(i\Delta_M - 2i\Delta_A - \frac{\kappa_m}{2} - \frac{\gamma}{2} - \frac{\Gamma_\phi}{2}\right) \hat{S}_{41}, \end{aligned} \quad (\text{A6i})$$

$$\begin{aligned} \dot{\hat{S}}_{42} = & \left[i(\Delta_M - \Delta_A) - \frac{\kappa_m}{2} - \gamma\right] \hat{S}_{42} + ig_s(\hat{c}^\dagger \hat{S}_{32} - \hat{S}_{41}\hat{c}) \\ & - ig_m \hat{S}_{43}. \end{aligned} \quad (\text{A6j})$$

We can derive the self-Kerr nonlinearity for the SAW phonon from Eq. (A6) by using the perturbation approach [60,75–77]. The operators can be expanded as $\hat{S}_{mn} = \hat{S}_{mn}^{(0)} + \hat{S}_{mn}^{(1)} + \hat{S}_{mn}^{(2)} + \hat{S}_{mn}^{(3)} + \dots$. In our configuration with $g_s \ll g_m$,

the system can be assumed in the ground state $|1\rangle$ to zeroth order, that is, $\hat{S}_{11}^{(0)} = 1, \hat{S}_{22}^{(0)} = \hat{S}_{33}^{(0)} = \hat{S}_{44}^{(0)} = 0$. The terms with $\hat{S}_{mn} g_s$ ($m \neq n$) can be neglected when solving \hat{S}_{mn} . Then we obtain the first-order solutions for the operators,

$$\hat{S}_{21}^{(1)} = -\frac{ig_s \hat{c}^\dagger}{g_m^2 F}, \quad (\text{A7a})$$

$$\hat{S}_{31}^{(1)} = -\frac{g_s \hat{c}^\dagger}{g_m F \left[-\frac{\kappa_m}{2} + i(\Delta_M - \Delta_A)\right]}, \quad (\text{A7b})$$

with

$$F = \frac{1}{\left[-\frac{\kappa_m}{2} + i(\Delta_M - \Delta_A)\right]} - \frac{\frac{\gamma}{2} + \frac{\Gamma_\phi}{2} + i\Delta_A}{g_m^2}. \quad (\text{A8})$$

As for a closed system, the total population is conserved, i.e., $\hat{S}_{11} + \hat{S}_{22} + \hat{S}_{33} + \hat{S}_{44} = 1$. The second-order diagonal elements satisfying the relationship,

$$\hat{S}_{11}^{(2)} + \hat{S}_{22}^{(2)} + \hat{S}_{33}^{(2)} + \hat{S}_{44}^{(2)} = 0. \quad (\text{A9})$$

Substituting Eqs. (A7) and (A9) to Eqs. (A6a)–(A6d), we obtain the second-order diagonal elements,

$$\hat{S}_{11}^{(2)} = -\frac{g_s^2 \hat{c}^\dagger \hat{c}}{g_m^2 \gamma} \left(\frac{1}{F} + \frac{1}{F^*}\right), \quad (\text{A10a})$$

$$\hat{S}_{22}^{(2)} = \frac{g_s^2 \hat{c}^\dagger \hat{c}}{g_m^2 \gamma} \left(\frac{1}{F} + \frac{1}{F^*}\right). \quad (\text{A10b})$$

Similarly, substituting Eqs. (A10) into Eq. (A6a)–(A6e), we obtain $\hat{S}_{21}^{(3)}$ to third order,

$$\hat{S}_{21}^{(3)} = -\frac{2ig_s^3 \hat{c}^\dagger \hat{c}^\dagger \hat{c}}{g_m^4 F \gamma} \left(\frac{1}{F} + \frac{1}{F^*}\right). \quad (\text{A11})$$

The first- and third-order approximations of $S_{43} = S_{43}^{(1)} + S_{43}^{(3)}$, $S_{43}^{(1)}$, and $S_{43}^{(3)}$ are zero. Using this perturbation approach, we get $S_{21} = S_{21}^{(1)} + S_{21}^{(3)}$. Substituting these formula for S_{21} into the Hamiltonian Eq. (A4), we obtain the effective Hamiltonian for the SAW phonon resonator only,

$$\hat{H}'_{\text{eff}} = (\tilde{\Delta} - \eta) \hat{c}^\dagger \hat{c} + \eta \hat{c}^\dagger \hat{c} \hat{c}^\dagger \hat{c}, \quad (\text{A12})$$

with an nonlinear interaction strength,

$$\eta = -g_s^2 F \left(\frac{1}{F^*} - \frac{1}{F}\right) \chi^{(3)} = \frac{2ig_s^4}{\gamma g_m^4} \left(\frac{1}{F^*} - \frac{1}{F}\right) \left(\frac{1}{F} + \frac{1}{F^*}\right), \quad (\text{A13})$$

due to the induced third-order polarization,

$$\chi^{(3)} = -\frac{2ig_s^2}{g_m^4 F \gamma} \left(\frac{1}{F} + \frac{1}{F^*}\right). \quad (\text{A14})$$

$\tilde{\Delta}$ is a linear shift and can be evaluated as

$$\tilde{\Delta} = \frac{g_s^2 \Delta_A}{g_m^2 \gamma} \left(\frac{1}{F} + \frac{1}{F^*}\right) + i \frac{g_s^2}{g_m^2} \left(\frac{1}{F^*} - \frac{1}{F}\right). \quad (\text{A15})$$

Throughout our investigation, we take $\Gamma_\phi = 0$.

Now we can consider the probe field with a central frequency ω_{in} . We define the second unitary transformation as

$$\hat{U}_2 = \exp\{i(\omega_{\text{in}} - \omega_A) \hat{c}^\dagger \hat{c} t\}, \quad (\text{A16})$$

the effective Hamiltonian of the system finally is represented by

$$\hat{H}_{\text{eff}} = (\bar{\Delta} - \eta - \Delta_a)\hat{c}^\dagger\hat{c} + \eta\hat{c}^\dagger\hat{c}\hat{c}^\dagger\hat{c} + i\sqrt{2\kappa_{p,e1}}\alpha_{\text{in}}(\hat{c}^\dagger - \hat{c}), \quad (\text{A17})$$

where $\Delta_a = \omega_{\text{in}} - \omega_A$. ω_{in} is the central frequency of the probe phonon wave packet. α_{in} corresponds to the amplitude of the weak coherent probe, and $\kappa_{p,e1}$ is the external loss of the SAW resonator due to the coupling to the input port. The coupling of the SAW phonon resonator to the output port also causes a decay rate $\kappa_{p,e2}$. We set $\kappa_{p,e1} = \kappa_{p,e2} = \kappa_{p,e}$. The SAW resonator decays at a total rate of $\kappa_p = \kappa_{p,i} + \kappa_{p,e1} + \kappa_{p,e2}$.

APPENDIX B: $g^2(0)$ IN THE WQR SYSTEM

Here we consider the WQR setup. In this case, a qubit couples to a SAW phonon mode propagating at a velocity v_g in a 1D SAW waveguide with a strength V ; see Fig. 1(b) in the main text. The qubit couples to a MW resonator. Similar to the RQR system, we can model the composite system consisting of the qubit and the MW resonator as an N-type 4LS as shown in Fig. 2(b). The SAW propagating in the waveguide drives the transitions of $|1\rangle \leftrightarrow |2\rangle$ and $|3\rangle \leftrightarrow |4\rangle$. The incident phonon coherent state is weak that we only need to consider the zero- and one-photon states in the MW resonator. The scattering of photons in the 1D photon waveguide by a 4LS controlled by a strong coherent light field has been studied in Refs. [68,87]. Here, we study the phonon scattering problem using the scattering matrix method [68,85,87] and show the bound-state resulted phonon blockade. In stark contrast to the previous photonic counterpart, the quantum vacuum field of the MW resonator plays the role of the coherent light field. Without an external driving in our system, the MW resonator is in its quantum vacuum state and the qubit in the ground state. The phonon bound state is created by the quantum vacuum-qubit coupling. Below, we mainly focus on the quantum phonon-phonon correlation induced by this bound state.

By linearizing the dispersion of the waveguide at the central frequency ω_{in} [84], we have the Hamiltonian for a moving SAW pulse coupling to the WQR system as

$$\begin{aligned} \hat{H} = & -i \int dx v_g \left[\hat{c}_R^\dagger(x) \frac{d}{dx} \hat{c}_R(x) - \hat{c}_L^\dagger(x) \frac{d}{dx} \hat{c}_L(x) \right] \\ & + (\bar{\Delta}_q - i\gamma)\hat{S}_{22} + (\bar{\Delta}_m - i\kappa_m)\hat{S}_{33} + (\Delta_4 - i\kappa_m - i\gamma)\hat{S}_{44} \\ & + \int dx V \delta(x) \{ [\hat{c}_R^\dagger(x) + \hat{c}_L^\dagger(x)] (\hat{S}_{12} + \hat{S}_{34}) + \text{H.c.} \} \\ & + g_m(\hat{S}_{23} + \hat{S}_{32}), \end{aligned} \quad (\text{B1})$$

with $\Delta_4 = (\bar{\Delta}_m + \bar{\Delta}_q)$. Where $\hat{c}_{R,L}^\dagger(x)$ are the creation operators for the right-going(left-going) phonon at x , $\bar{\Delta}_m = \omega_m - \omega_{\text{in}}$, and $\bar{\Delta}_q = \omega_e - \omega_{\text{in}}$. The rate of the spontaneous emission of the qubit to the 1D waveguide is given by $\Gamma = V^2/v_g$ [85].

Transforming the right- (left)-moving modes to even (odd) modes:

$$\hat{c}_e^\dagger(x) = \frac{\hat{c}_R^\dagger(x) + \hat{c}_L^\dagger(-x)}{\sqrt{2}}, \quad (\text{B2a})$$

$$\hat{c}_o^\dagger(x) = \frac{\hat{c}_R^\dagger(x) - \hat{c}_L^\dagger(-x)}{\sqrt{2}}. \quad (\text{B2b})$$

Under these two decoupled modes, the Hamiltonian becomes

$$\hat{H} = \hat{H}_e + \hat{H}_o, \quad (\text{B3a})$$

$$\begin{aligned} \hat{H}_e = & -i \int dx v_g \hat{c}_e^\dagger(x) \frac{d}{dx} \hat{c}_e(x) \\ & + \int dx \sqrt{2V} \delta(x) \{ \hat{c}_e^\dagger(x) (\hat{S}_{12} + \hat{S}_{34}) + \text{H.c.} \} \\ & + (\bar{\Delta}_q - i\gamma)\hat{S}_{22} + (\bar{\Delta}_m - i\kappa_m)\hat{S}_{33} \\ & + (\Delta_4 - i\kappa_m - i\gamma)\hat{S}_{44} + g_m(\hat{S}_{23} + \hat{S}_{32}), \end{aligned} \quad (\text{B3b})$$

$$\hat{H}_o = -i \int dx v_g \hat{c}_o^\dagger(x) \frac{d}{dx} \hat{c}_o(x). \quad (\text{B3c})$$

Since the total number of excitations in both the even and odd spaces are separately conserved [68], we mainly focus on finding the nontrivial even-mode solution and then transform back to the left-right representation. The n-excitation state in the even space is given by

$$\begin{aligned} |\psi_n\rangle_e = & \left[\int dx^n \phi^{(n)} \hat{c}_e^\dagger(x_1) \cdots \hat{c}_e^\dagger(x_n) \right. \\ & + \int dx^{n-1} \sum_{j=2,3} f_j^{(n)} \hat{S}_{j1} \hat{c}_e^\dagger(x_1) \cdots \hat{c}_e^\dagger(x_{n-1}) \\ & \left. + \int dx^{n-2} f_4^{(n)} \hat{S}_{41} \hat{c}_e^\dagger(x_1) \cdots \hat{c}_e^\dagger(x_{n-2}) \right] |\emptyset, 1\rangle, \end{aligned} \quad (\text{B4})$$

where $|\emptyset, 1\rangle$ is the zero-phonon state with the 4LS in the state $|1\rangle$. The scattering eigenstates are constructed by imposing the open boundary condition that $\phi^{(n)}(x_1, \dots, x_n)$ is a free plane wave in the incident region $x_1, \dots, x_n < 0$ [88]. Then we can obtain the scattering of one- and two-phonon eigenstates following Refs. [68,87,89].

The one-phonon eigenstate with eigenenergy $E = v_g k$ and wave vector k , and the transmission amplitude are

$$\phi^{(1)}(x) = \phi_k(x) = \frac{e^{ikx}}{\sqrt{2\pi}} [\theta(-x) + \bar{t}_k \theta(x)], \quad (\text{B5a})$$

$$\bar{t}_k = \frac{(v_g k - \bar{\Delta}_m + i\kappa_m)[v_g k - \bar{\Delta}_q + i(\gamma - \Gamma)] - g_m^2}{(v_g k - \bar{\Delta}_m + i\kappa_m)[v_g k - \bar{\Delta}_q + i(\gamma + \Gamma)] - g_m^2}, \quad (\text{B5b})$$

where $\theta(x)$ is the step function. For the two-phonon eigenstate with eigenenergy $E = v_g(k_1 + k_2)$ and wave vectors k_1 and k_2 of the two phonons, the wave function and bound state are

$$\begin{aligned} \phi^{(2)}(x_1, x_2) = & \frac{1}{2} \sum_Q \phi_{k_1}(x_{Q_1}) \phi_{k_2}(x_{Q_2}) \\ & + \frac{1}{2} \sum_{P,Q} B_{k_{P_1}, k_{P_2}}(x_{Q_1}, x_{Q_2}) \theta(x_{Q_1}), \end{aligned} \quad (\text{B6a})$$

$$B_{k_{P_1}, k_{P_2}}(x_{Q_1}, x_{Q_2}) = e^{iE x_{Q_2}} \sum_{j=1,2} C_j e^{-\mu_j |x_2 - x_1|} \theta(x_{Q_2} - x_{Q_1}), \quad (\text{B6b})$$

where $P = \{P_1, P_2\}$ and $Q = \{Q_1, Q_2\}$, and

$$\begin{aligned}
v_g \mu_1 &= \frac{\Gamma + \gamma + \kappa_m}{2} - \xi - i \left(\frac{\Delta_M}{2} - \bar{\Delta}_q - \vartheta \right), \\
v_g \mu_2 &= \frac{\Gamma + \gamma + \kappa_m}{2} + \xi + i \left(\frac{\Delta_M}{2} + \bar{\Delta}_q + \vartheta \right), \\
\xi &= \frac{\sqrt{2}}{4} \left(\sqrt{\chi^2 - 4\Delta_M^2 \Gamma_p^2} - \chi \right)^{\frac{1}{2}}, \\
\vartheta &= \frac{\sqrt{2}}{4} \left(\sqrt{\chi^2 - 4\Delta_M^2 \Gamma_p^2} + \chi \right)^{\frac{1}{2}}, \\
\chi &= \Delta_M^2 + 4g_m^2 - \Gamma_p^2, \\
\Gamma_p &= \Gamma + \gamma - \kappa_m, \\
C_1 &= \frac{\beta - \alpha \lambda_2}{\lambda_1 - \lambda_2}, \\
C_2 &= \frac{-\beta + \alpha \lambda_1}{\lambda_1 - \lambda_2}, \\
\lambda_1 &= \frac{\Gamma_p}{2} + \xi - i \left(\frac{\Delta_M}{2} - \vartheta \right), \\
\lambda_2 &= \frac{\Gamma_p}{2} - \xi - i \left(\frac{\Delta_M}{2} + \vartheta \right), \\
\beta &= \frac{\Gamma g_m^2}{2\pi} \left(\frac{\bar{i}_{k_1} - v}{\rho_{k_2}} + \frac{\bar{i}_{k_2} - v}{\rho_{k_1}} \right), \\
\alpha &= -\frac{(\bar{i}_{k_1} - 1)(\bar{i}_{k_2} - 1)}{2\pi}, \\
v &= \frac{\bar{\Delta}_m + \bar{\Delta}_q - E - i(\kappa_m + \gamma - \Gamma)}{\bar{\Delta}_m + \bar{\Delta}_q - E - i(\kappa_m + \gamma + \Gamma)}, \\
\rho_{k_1} &= (v_g k_1 - \bar{\Delta}_q - \Delta_M + i\kappa_m) \\
&\quad \times [v_g k_1 - \bar{\Delta}_q + i(\gamma + \Gamma)] - g_m^2, \\
\rho_{k_2} &= (v_g k_2 - \bar{\Delta}_q - \Delta_M + i\kappa_m) \\
&\quad \times [v_g k_2 - \bar{\Delta}_q + i(\gamma + \Gamma)] - g_m^2. \tag{B7}
\end{aligned}$$

We consider a right-moving incident phonon. In our case, the microwave resonator is in its quantum vacuum state and the qubit in the ground state. The incident phonon state is a wave packet, and can be described by the continuous-mode phonon creation operator as

$$\hat{c}_{R,L}^\dagger = \int dk \alpha(k) \hat{c}_{R,L}^\dagger(k), \tag{B8}$$

where the amplitude $\alpha(k)$ satisfies the normalization condition $\int dk |\alpha(k)|^2 = 1$. The corresponding continuous-mode n-phonon Fock state is

$$|n\rangle_{R,L} = \frac{(\hat{c}_{R,L}^\dagger)^n}{\sqrt{n!}} |\emptyset\rangle. \tag{B9}$$

From the scattering eigenstates, we can construct the scattering matrices [89]. Applying the scattering matrices on the

incident phonon states, we can then obtain the scattering one-phonon state,

$$|\psi^{(1)}\rangle = \int dk \alpha(k) (t_k \hat{c}_R^\dagger(k) + r_k \hat{c}_L^\dagger(k)) |\emptyset\rangle, \tag{B10a}$$

$$t_k = (\bar{i}_k + 1)/2, \quad r_k = (\bar{i}_k - 1)/2, \tag{B10b}$$

and the scattering two-phonon state,

$$\begin{aligned}
|\psi^{(2)}\rangle &= \int dk_1 dk_2 dx_1 dx_2 \frac{1}{\sqrt{2}} \alpha(k_1) \alpha(k_2) \\
&\quad \times \left[\frac{1}{2} t_{k_1, k_2}(x_1, x_2) \hat{c}_R^\dagger(x_1) \hat{c}_R^\dagger(x_2) \right. \\
&\quad + \Xi_{k_1, k_2}(x_1, -x_2) \hat{c}_R^\dagger(x_1) \hat{c}_L^\dagger(x_2) \\
&\quad \left. + \frac{1}{2} r_{k_1, k_2}(-x_1, -x_2) \hat{c}_L^\dagger(x_1) \hat{c}_L^\dagger(x_2) \right] |\emptyset\rangle, \tag{B11}
\end{aligned}$$

with

$$\begin{aligned}
t_{k_1, k_2} &= \frac{1}{2\pi} t_{k_1} t_{k_2} e^{ik_1 x_1 + k_2 x_2} \\
&\quad + \frac{1}{4} B_{k_1, k_2}(x_1, x_2) + (k_1 \leftrightarrow k_2), \\
\Xi_{k_1, k_2} &= \frac{1}{2\pi} t_{k_1} r_{k_2} e^{ik_1 x_1 + k_2 x_2} \\
&\quad + \frac{1}{4} B_{k_1, k_2}(x_1, x_2) + (k_1 \leftrightarrow k_2), \\
r_{k_1, k_2} &= \frac{1}{2\pi} r_{k_1} r_{k_2} e^{ik_1 x_1 + k_2 x_2} \\
&\quad + \frac{1}{4} B_{k_1, k_2}(x_1, x_2) + (k_1 \leftrightarrow k_2), \\
B_{k_1, k_2}(x_1, x_2) &= e^{i(k_1 + k_2)x_2} \sum_{j=1,2} C_j e^{-\mu_j |x_2 - x_1|} \theta(x_{Q_2} - x_{Q_1}) \\
&\quad + (x_1 \leftrightarrow x_2). \tag{B12}
\end{aligned}$$

t_{k_1, k_2} and r_{k_1, k_2} represent the two-phonon transmission coefficient and two-phonon reflection, respectively. Ξ_{k_1, k_2} is the coefficient for the one-phonon transmitted and one-phonon reflected. $B_{k_1, k_2}(x_{Q_1}, x_{Q_2})$ describes the phonon bound state. The denotation $k_1 \leftrightarrow k_2$ ($x_1 \leftrightarrow x_2$) means to exchange k_1 and k_2 (x_1 and x_2) [87].

From the scattering state $|\psi\rangle = |\psi^{(1)}\rangle + |\psi^{(2)}\rangle$, we can calculate the second-order correlation function $g^{(2)}(0)$ of the transmitted SAW through the N-type system with the formula [87],

$$g^{(2)}(0) = \frac{\langle \psi | \hat{c}_R^\dagger(x) \hat{c}_R^\dagger(x) \hat{c}_R(x) \hat{c}_R(x) | \psi \rangle}{|\langle \psi | \hat{c}_R^\dagger(x) \hat{c}_R(x) | \psi \rangle|^2}. \tag{B13}$$

Substituting Eq. (B10) and Eq. (B11) into Eq. (B13), we can obtain

$$g^{(2)}(0) = \frac{|\int dk_1 dk_2 \alpha(k_1) \alpha(k_2) (t_{k_1} t_{k_2} - B)|^2}{|\int dk_1 dk_2 \alpha(k_1) \alpha(k_2) t_{k_1} t_{k_2}|^2}, \tag{B14a}$$

$$B = \pi(C_1 + C_2) = -2r_{k_1} r_{k_2}. \tag{B14b}$$

In the numerator, the first term comes from the plane wave (PW), and the second one is the contribution of the bound state (BS).

- [1] J. Q. You and F. Nori, *Phys. Today* **58**(11), 42 (2005).
- [2] G. Wendin, *Rep. Prog. Phys.* **80**, 106001 (2017).
- [3] M. H. Devoret and R. J. Schoelkopf, *Science* **339**, 1169 (2013).
- [4] F. Arute *et al.*, *Nature (London)* **574**, 505 (2019).
- [5] M. Gong, M.-C. Chen, Y. Zheng, S. Wang, C. Zha, H. Deng, Z. Yan, H. Rong, Y. Wu, S. Li, F. Chen, Y. Zhao, F. Liang, J. Lin, Y. Xu, C. Guo, L. Sun, A. D. Castellano, H. Wang, C. Peng, C.-Y. Lu, X. Zhu, and J.-W. Pan, *Phys. Rev. Lett.* **122**, 110501 (2019).
- [6] Y. Zheng, C. Song, M.-C. Chen, B. Xia, W. Liu, Q. Guo, L. Zhang, D. Xu, H. Deng, K. Huang, Y. Wu, Z. Yan, D. Zheng, L. Lu, J.-W. Pan, H. Wang, C.-Y. Lu, and X. Zhu, *Phys. Rev. Lett.* **118**, 210504 (2017).
- [7] P. Zhang, Y. D. Wang, and C. P. Sun, *Phys. Rev. Lett.* **95**, 097204 (2005).
- [8] K. Xia and J. Evers, *Phys. Rev. Lett.* **103**, 227203 (2009).
- [9] K. Xia and J. Evers, *Phys. Rev. B* **82**, 184532 (2010).
- [10] Z. Yan, Y.-R. Zhang, M. Gong, Y. Wu, Y. Zheng, S. Li, C. Wang, F. Liang, J. Lin, Y. Xu, C. Guo, L. Sun, C.-Z. Peng, K. Xia, H. Deng, H. Rong, J. Q. You, F. Nori, H. Fan, X. Zhu, and J.-W. Pan, *Science* **364**, 753 (2019).
- [11] C. Song, K. Xu, W. Liu, C.-P. Yang, S.-B. Zheng, H. Deng, Q. Xie, K. Huang, Q. Guo, L. Zhang, P. Zhang, D. Xu, D. Zheng, X. Zhu, H. Wang, Y.-A. Chen, C.-Y. Lu, S. Han, and J.-W. Pan, *Phys. Rev. Lett.* **119**, 180511 (2017).
- [12] A. Cho, *Science* **359**, 1202 (2018).
- [13] M. J. A. Schuetz, E. M. Kessler, G. Giedke, L. M. K. Vandersypen, M. D. Lukin, and J. I. Cirac, *Physical Review X* **5**, 031031 (2015).
- [14] M. Kervinen, I. Rissanen, and M. Sillanpää, *Phys. Rev. B* **97**, 205443 (2018).
- [15] B. A. Moores, L. R. Sletten, J. J. Viennot, and K. W. Lehnert, *Phys. Rev. Lett.* **120**, 227701 (2018).
- [16] X. Han, C.-L. Zou, and H. X. Tang, *Phys. Rev. Lett.* **117**, 123603 (2016).
- [17] A. Noguchi, R. Yamazaki, Y. Tabuchi, and Y. Nakamura, *Phys. Rev. Lett.* **119**, 180505 (2017).
- [18] V. S. Shumeiko, *Phys. Rev. A* **93**, 023838 (2016).
- [19] Y. Chu, P. Kharel, W. H. Renninger, L. D. Burkhardt, L. Frunzio, P. T. Rakich, and R. J. Schoelkopf, *Science* **358**, 199 (2017).
- [20] M. V. Gustafsson, T. Aref, A. F. Kockum, M. K. Ekström, G. Johansson, and P. Delsing, *Science* **346**, 207 (2014).
- [21] J. Koch, T. M. Yu, J. Gambetta, A. A. Houck, D. I. Schuster, J. Majer, A. Blais, M. H. Devoret, S. M. Girvin, and R. J. Schoelkopf, *Phys. Rev. A* **76**, 042319 (2007).
- [22] A. A. Houck, J. A. Schreier, B. R. Johnson, J. M. Chow, J. Koch, J. M. Gambetta, D. I. Schuster, L. Frunzio, M. H. Devoret, S. M. Girvin, and R. J. Schoelkopf, *Phys. Rev. Lett.* **101**, 080502 (2008).
- [23] J. A. Schreier, A. A. Houck, J. Koch, D. I. Schuster, B. R. Johnson, J. M. Chow, J. M. Gambetta, J. Majer, L. Frunzio, M. H. Devoret, S. M. Girvin, and R. J. Schoelkopf, *Phys. Rev. B* **77**, 180502(R) (2008).
- [24] Z.-L. Xiang, S. Ashhab, J. Q. You, and F. Nori, *Reviews of Modern Physics* **85**, 623 (2013).
- [25] D. Ristè, C. C. Bultink, M. J. Tiggelman, R. N. Schouten, K. W. Lehnert, and L. DiCarlo, *Nat. Commun.* **4**, 1913 (2013).
- [26] Y. Ye, Z.-Y. Ge, Y. Wu, S. Wang, M. Gong, Y.-R. Zhang, Q. Zhu, R. Yang, S. Li, F. Liang, J. Lin, Y. Xu, C. Guo, L. Sun, C. Cheng, N. Ma, Z. Y. Meng, H. Deng, H. Rong, C.-Y. Lu, C.-Z. Peng, H. Fan, X. Zhu, and J.-W. Pan, *Phys. Rev. Lett.* **123**, 050502 (2019).
- [27] A. N. Bolgar, J. I. Zotova, D. D. Kirichenko, I. S. Besedin, A. V. Semenov, R. S. Shaikhaidarov, and O. V. Astafiev, *Phys. Rev. Lett.* **120**, 223603 (2018).
- [28] R. Manenti, A. F. Kockum, A. Patterson, T. Behrle, J. Rahamim, G. Tancredi, F. Nori, and P. J. Leek, *Nat. Commun.* **8**, 975 (2017).
- [29] Y. Chu, P. Kharel, T. Yoon, L. Frunzio, P. T. Rakich, and R. J. Schoelkopf, *Nature (London)* **563**, 666 (2018).
- [30] K. J. Satzinger, Y. P. Zhong, H. S. Chang, G. A. Peairs, A. Bienfait, M.-H. Chou, A. Y. Cleland, C. R. Conner, É. Dumur, J. Grebel, I. Gutierrez, B. H. November, R. G. Povey, S. J. Whiteley, D. D. Awschalom, D. I. Schuster, and A. N. Cleland, *Nature (London)* **563**, 661 (2018).
- [31] I. Lekavicius, D. A. Golter, T. Oo, and H. Wang, *Phys. Rev. Lett.* **119**, 063601 (2017).
- [32] D. A. Golter, T. Oo, M. Amezcua, I. Lekavicius, K. A. Stewart, and H. Wang, *Phys. Rev. X* **6**, 041060 (2016).
- [33] M. Fleischhauer, A. Imamoglu, and J. P. Marangos, *Rev. Mod. Phys.* **77**, 633 (2005).
- [34] Y.-F. Jiao, T.-X. Lu, and H. Jing, *Phys. Rev. A* **97**, 013843 (2018).
- [35] Q.-T. Cao, H. Wang, C.-H. Dong, H. Jing, R.-S. Liu, X. Chen, L. Ge, Q. Gong, and Y.-F. Xiao, *Phys. Rev. Lett.* **118**, 033901 (2017).
- [36] K. Xia, F. Nori, and M. Xiao, *Phys. Rev. Lett.* **121**, 203602 (2018).
- [37] B. Dayan, A. S. Parkins, T. Aoki, E. P. Ostby, K. J. Vahala, and H. J. Kimble, *Science* **319**, 1062 (2008).
- [38] A. Imamoglu, H. Schmidt, G. Woods, and M. Deutsch, *Phys. Rev. Lett.* **79**, 1467 (1997).
- [39] M. J. Werner and A. Imamoglu, *Phys. Rev. A* **61**, 011801(R) (1999).
- [40] S. Rebić, A. S. Parkins, and S. M. Tan, *Phys. Rev. A* **65**, 063804 (2002).
- [41] C. Hamsen, K. N. Tolazzi, T. Wilk, and G. Rempe, *Nat. Phys.* **14**, 885 (2018).
- [42] R. Huang, A. Miranowicz, J.-Q. Liao, F. Nori, and H. Jing, *Phys. Rev. Lett.* **121**, 153601 (2018).
- [43] R. Trivedi, M. Radulaski, K. A. Fischer, S. Fan, and J. Vučković, *Phys. Rev. Lett.* **122**, 243602 (2019).
- [44] S. Ding, G. Maslennikov, R. Hablützel, and D. Matsukevich, *Phys. Rev. Lett.* **119**, 193602 (2017).
- [45] Y.-x. Liu, A. Miranowicz, Y. B. Gao, J. Bajer, C. P. Sun, and F. Nori, *Phys. Rev. A* **82**, 032101 (2010).
- [46] N. Didier, S. Pugnetti, Y. M. Blanter, and R. Fazio, *Phys. Rev. B* **84**, 054503 (2011).
- [47] X. Wang, A. Miranowicz, H.-R. Li, and F. Nori, *Phys. Rev. A* **93**, 063861 (2016).
- [48] L.-L. Zheng, T.-S. Yin, Q. Bin, X.-Y. Lü, and Y. Wu, *Phys. Rev. A* **99**, 013804 (2019).
- [49] H. Xie, C.-G. Liao, X. Shang, M.-Y. Ye, and X.-M. Lin, *Phys. Rev. A* **96**, 013861 (2017).
- [50] A. Miranowicz, J. Bajer, N. Lambert, Y.-X. Liu, and F. Nori, *Phys. Rev. A* **93**, 013808 (2016).
- [51] K. Cai, Z.-W. Pan, R.-X. Wang, D. Ruan, Z.-Q. Yin, and G.-L. Long, *Opt. Lett.* **43**, 1163 (2018).
- [52] H. Schmidt and A. Imamoglu, *Opt. Lett.* **21**, 1936 (1996).
- [53] H. Kang and Y. Zhu, *Phys. Rev. Lett.* **91**, 093601 (2003).

- [54] H. Schmidt and A. R. Hawkins, *Appl. Phys. Lett.* **86**, 032106 (2005).
- [55] M. D. Lukin and A. Imamoglu, *Phys. Rev. Lett.* **84**, 1419 (2000).
- [56] S. Rebić, J. Twamley, and G. J. Milburn, *Phys. Rev. Lett.* **103**, 150503 (2009).
- [57] S. Rebić, S. M. Tan, A. S. Parkins, and D. F. Walls, *J. Opt. B: Quantum Semiclass. Opt.* **1**, 490 (1999).
- [58] X. Yang, K. Ying, Y. Niu, and S. Gong, *J. Opt.* **17**, 045505 (2015).
- [59] H.-Y. Lo, Y.-C. Chen, P.-C. Su, H.-C. Chen, J.-X. Chen, Y.-C. Chen, I. A. Yu, and Y.-F. Chen, *Phys. Rev. A* **83**, 041804(R) (2011).
- [60] J. Sheng, X. Yang, H. Wu, and M. Xiao, *Phys. Rev. A* **84**, 053820 (2011).
- [61] J. Evers, M. Kiffner, M. Macovei, and C. H. Keitel, *Phys. Rev. A* **73**, 023804 (2006).
- [62] M. Kiffner, M. Macovei, J. Evers, and C. Keitel, *Progress in Optics*, Vol. 55 (Elsevier, Amsterdam, 2010), pp. 85–197.
- [63] I.-C. Bena-Chelmus, F. F. Settembrini, G. Scalari, and J. Faist, *Nature (London)* **568**, 202 (2019).
- [64] I.-C. Hoi, A. Kockum, L. Tornberg, A. Pourkabirian, G. Johansson, P. Delsing, and C. Wilson, *Nat. Phys.* **11**, 1045 (2015).
- [65] C. Riek, D. V. Seletskiy, A. S. Moskalenko, J. F. Schmidt, P. Krauspe, S. Eckart, S. Eggert, G. Burkard, and A. Leitenstorfer, *Science* **350**, 420 (2015).
- [66] H. Tanji-Suzuki, W. Chen, R. Landig, J. Simon, and V. Vuletić, *Science* **333**, 1266 (2011).
- [67] K. Y. Fong, H.-K. Li, R. Zhao, S. Yang, Y. Wang, and X. Zhang, *Nature (London)* **576**, 243 (2019).
- [68] H. Zheng, D. J. Gauthier, and H. U. Baranger, *Phys. Rev. Lett.* **107**, 223601 (2011).
- [69] P. Krantz, M. Kjaergaard, F. Yan, T. P. Orlando, S. Gustavsson, and W. D. Oliver, *Appl. Phys. Rev.* **6**, 021318 (2019).
- [70] J. M. Fink, R. Bianchetti, M. Baur, M. Göppl, L. Steffen, S. Filipp, P. J. Leek, A. Blais, and A. Wallraff, *Phys. Rev. Lett.* **103**, 083601 (2009).
- [71] A. A. Houck, J. Koch, M. H. Devoret, S. M. Girvin, and R. J. Schoelkopf, *Quant. Info. Proc.* **8**, 105 (2009).
- [72] J. Li, M. P. Silveri, K. S. Kumar, J. M. Pirkkalainen, A. Vepsäläinen, W. C. Chien, J. Tuorila, M. A. Sillanpää, P. J. Hakonen, E. V. Thuneberg, and G. S. Paraoanu, *Nat. Commun.* **4**, 1420 (2013).
- [73] J. A. Mlynek, A. A. Abdumalikov, C. Eichler, and A. Wallraff, *Nat. Commun.* **5**, 5186 (2014).
- [74] P. R. Rice and R. J. Brecha, *Opt. Commun.* **126**, 230 (1996).
- [75] Y.-q. Li and M. Xiao, *Phys. Rev. A* **51**, R2703 (1995).
- [76] K. Okamoto, *Fundamentals of Optical Waveguides* (Academic Press, Cambridge, 2006).
- [77] M. O. Scully, M. S. Zubairy *et al.*, *Quantum Optics* (Cambridge University Press, Cambridge, 1997).
- [78] C. W. Gardiner and M. J. Collett, *Phys. Rev. A* **31**, 3761 (1985).
- [79] M. V. Gustafsson, P. V. Santos, G. Johansson, and P. Delsing, *Nat. Phys.* **8**, 338 (2012).
- [80] M. K. Ekström, T. Aref, J. Runeson, J. Björck, I. Boström, and P. Delsing, *Appl. Phys. Lett.* **110**, 073105 (2017).
- [81] M. K. Ekström, T. Aref, A. Ask, G. Andersson, B. Suri, H. Sanada, G. Johansson, and P. Delsing, *New J. Phys.* **21**, 123013 (2019).
- [82] I.-C. Hoi, C. M. Wilson, G. Johansson, T. Palomaki, B. Peropadre, and P. Delsing, *Phys. Rev. Lett.* **107**, 073601 (2011).
- [83] I.-C. Hoi, T. Palomaki, J. Lindkvist, G. Johansson, P. Delsing, and C. M. Wilson, *Phys. Rev. Lett.* **108**, 263601 (2012).
- [84] J. T. Shen and S. Fan, *Opt. Lett.* **30**, 2001 (2005).
- [85] J.-T. Shen and S. Fan, *Phys. Rev. A* **79**, 023837 (2009).
- [86] D. Roy, C. M. Wilson, and O. Firstenberg, *Rev. Mod. Phys.* **89**, 021001 (2017).
- [87] H. Zheng, D. J. Gauthier, and H. U. Baranger, *Phys. Rev. A* **85**, 043832 (2012).
- [88] A. Nishino, T. Imamura, and N. Hatano, *Phys. Rev. Lett.* **102**, 146803 (2009).
- [89] H. Zheng, D. J. Gauthier, and H. U. Baranger, *Phys. Rev. A* **82**, 063816 (2010).
- [90] A. Bienfait, K. J. Satzinger, Y. P. Zhong, H.-S. Chang, M.-H. Chou, C. R. Conner, É. Dumur, J. Grebel, G. A. Peairs, R. G. Povey, and A. N. Cleland, *Science* **364**, 368 (2019).
- [91] K. M. Birnbaum, A. Boca, R. Miller, A. D. Boozer, T. E. Northup, and H. J. Kimble, *Nature (London)* **436**, 87 (2005).
- [92] J. Zhou, X. Tao, J. Luo, Y. Li, H. J. S. Dong, J. Luo, H. Duan, and Y. Fu, *Surf. Coat. Technol.* **367**, 127 (2019).
- [93] S. J. Whiteley, G. Wolfowicz, C. P. Anderson, A. Bourassa, H. Ma, M. Ye, G. Koolstra, K. J. Satzinger, M. V. Holt, F. J. Heremans, A. N. Cleland, D. I. Schuster, G. Galli, and D. D. Awschalom, *Nat. Phys.* **15**, 490 (2019).
- [94] F. Yoshihara, T. Fuse, S. Ashhab, K. Kakuyanagi, S. Saito, and K. Semba, *Nat. Phys.* **13**, 44 (2017).
- [95] D. F. Walls and G. J. Milburn, *Quantum Optics* (Springer Science & Business Media, Berlin, Heidelberg, 2007).
- [96] M. Lewenstein, A. Sanpera, and M. Pospiech, *Quantum Optics: An Introduction* (University of Hannover, Germany, 2006).
- [97] K. Xia, N. Zhao, and J. Twamley, *Phys. Rev. A* **92**, 043409 (2015).